Buckling and snapping of elastic beams

THESIS

submitted in partial fulfillment of the
requirements for the degree of

BACHELOR OF SCIENCE
in
PHYSICS AND MATHEMATICS

Author :	Mara Smeele
Student ID :	1141171
Supervisors Physics :	Prof. dr. Martin van Hecke
	Dr. Corentin Coulais
	MSc. Luuk Lubbers
Supervisor Mathematics :	Dr. Vivi Rottschäfer

Leiden, The Netherlands, July 16, 2015

Buckling and snapping of elastic beams

Mara Smeele

Huygens-Kamerlingh Onnes Laboratory, Leiden University
P.O. Box 9500, 2300 RA Leiden, The Netherlands
Mathematical Institute Leiden, Leiden University
P.O. Box 9512, 2300 RA Leiden, The Netherlands

July 16, 2015

Abstract

This thesis is a study on the many instabilities of one-dimensional beams with a force and a moment applied on the endpoints. The static equilibrium states of a beam can be found by energy minimization, resulting in a nonlinear inhomogeneous differential equation, which we solve analytically. We explore the behaviour of the beams and the instabilities. When a confining force is applied to an initially straight beam, a symmetric pitchfork bifurcation, also called Euler buckling, occurs. Then, when a moment is applied, or for beams with a constant pre-curvature, the symmetry is broken and the buckling instability disappears. An unfolded pitchfork bifurcation seeds a new snapping instability, controlled by the moment at the endpoints. For higher modes the same scenario repeats. This suggests the system then undergoes a sequence of cusp catastrophes.

Contents

Chapter 1

Introduction

For my bachelor thesis I was searching for a subject that is suitable for both mathematics and physics. I chose to study elastic beams and continue the work of Willem Schouten, who did his bachelor thesis on this subject in 2014. How is it possible to work so long on beams? Well that's easy. It is very interesting and I would like to learn even more about beams. Fascinating that beams are already studied for centuries!

What are the limits of describing a one-dimensional beam in a continuous way? In other words

How far can we push the elastica keeping the model continuous?

Elastica is the study of thin elastic lines. In the 13th century Jordanus de Nemore was the first who studied elastica. In the 17e century Euler developed a mathematical theory for the buckling of elastic beams [1]. A beam is a slender object whose width is much smaller than its length. Euler studied initially straight beams with a force applied on the endpoints of the beam. First the beam remains straight and at a critical force, $\overline{P}_c$, the beam buckles into one of the two directions, as shown in figure 1.1. This buckling process is called Euler buckling [2].

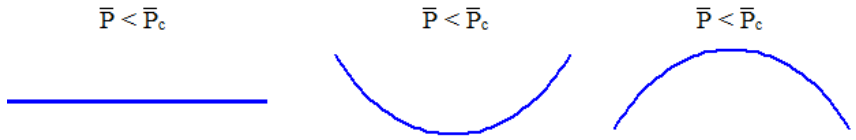

Figure 1.1: *Euler buckling. The beam is straight for $\overline{P} < \overline{P}_c$ and buckled into one of the two directions for $\overline{P} > \overline{P}_c$.*

Our interest in the elastica comes from the study of elastic materials. An example of an elastic material is a Holey sheet, a sheet of elastic material with a regular pattern of holes. The first ones who came up with a Holey sheet were Mullin et al. [3]. They designed a Monoholar sheet. This is a Holey sheet with circular holes of equal size, see figure 1.2. Under compression, most materials shrink into the direction of compressing and extend into the other directions. These materials have a positive Poisson's ratio. The Poisson's ratio, ν, is given by the following formula

$$\nu = -\frac{\text{lateral strain}}{\text{axial strain}}. \tag{1.1}$$

Strain is defined as the elongation per unit length [4]. A special property of the Monoholar sheet is that under compression it shrinks into the transverse directions, see figure 1.2. This effect is a negative Poisson's ratio [5]. Under compression the circular holes become elliptical. This pattern transformation is a symmetry breaking instability: the orientation of the ellipses is unpredictable [3].

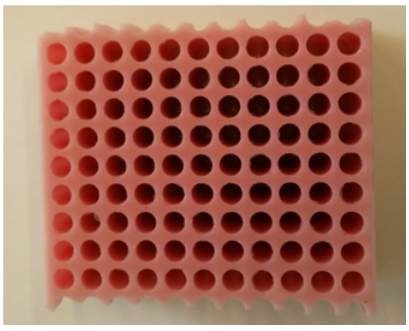

Monoholar sheet before compression. A regular pattern of circular holes.

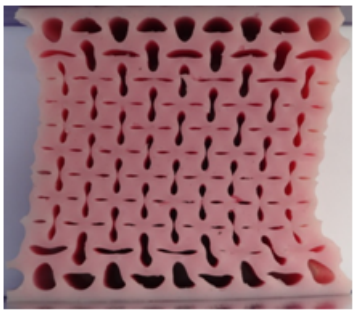

Compressed Monoholar sheet, with negative Poisson's ratio. The holes have become ellipses.

Figure 1.2: *Monoholar sheet before and after compression [3].*

A Monoholar sheet can be modelled by a network of blocks connected by initially straight beams, see figure 1.3. Under compression the beams first remain straight and at a critical force the beams buckle into one of the two directions, like the ellipses. So in a Monoholar sheet find see beam buckling. The beams in a Monoholar sheet stay symmetric after deformation. In this thesis we model a beam by an one-dimensional beam and apply a force at the endpoints of the beam, see figure 1.4.

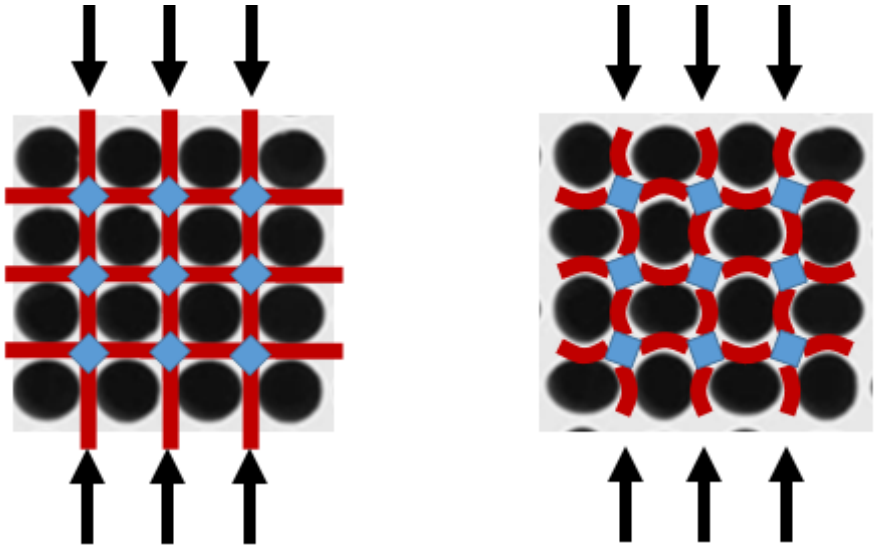

Model of Monoholar sheet for $\overline{P} < \overline{P}_c$. *Model of Monoholar sheet for $\overline{P} > \overline{P}_c$.*

Figure 1.3: *Monoholar sheet modelled by a network of blocks connected by beams. The blue squares are the blocks and the red bars are the beams. The arrows point in the direction of the applied force.*

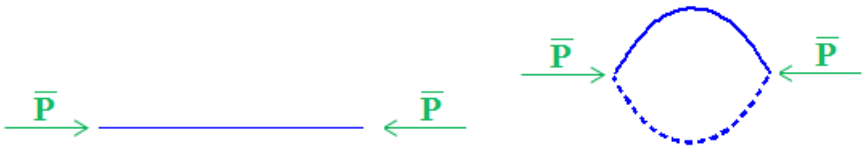

One-dimensional beam for $\overline{P} < \overline{P}_c$ *For $\overline{P} > \overline{P}_c$ the beam buckles into one of the two directions.*

Figure 1.4: *One-dimensional beam with a force, $\overline{P}$, applied on the endpoints.*

Figure 1.5 shows another holey sheet. This sheet has two different hole sizes and is called a Biholar sheet.

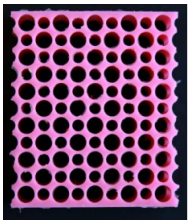

Figure 1.5: *Biholar sheet in its initial position [6].*

Apart from a negative Poisson's ratio the Biholar sheet has other special properties. Figure 1.6 shows a Biholar sheet with clamps. These clamps impose a compression in the transverse direction. Then the material is compressed in the vertical direction. The amount of compression of these clamps influences the stiffness of the material. Therefore the Biholar sheet is a programmable material. When the material is compressed the holes become elliptical, the orientation depends on the competition between the horizontal and vertical compression. During the compression an ellipse can have two different orientations, see figure 1.6 [6].

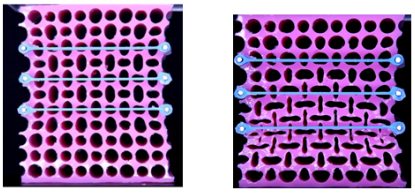

Biholar sheet with clamps. The ellipses have two possible orientations.

Zoom of a fiew holes to have a better view at the two possible orientations.

Figure 1.6: *During compression the holes have two different orientations [6].*

A Biholar sheet can also be modelled by a network of blocks connected by beams, which stay symmetric after deformation. Only now the beams are pre-curved. When the material is compressed the beams bend and at a certain force they switch orientation, this is called snapping. We model this by an one-dimensional beam and apply a force and a moment at the endpoints of the beam, see figure 1.7. We apply a moment because the force applied on the blocks applies a torque on the beam.

One-dimensional pre-curved beam in its initial position.

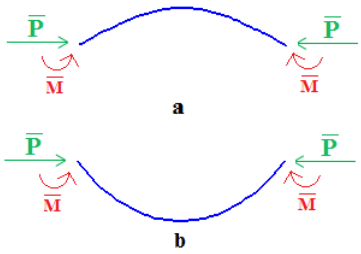

Snapping of the beam from state a to state b.

Figure 1.7: *One-dimensional beam with a force and a moment applied on the endpoints.*

This thesis is a study on continuous one-dimensional beams. On these beams we apply a moment and a force at the endpoints and explore the various instabilities they undergo. The boundary conditions we impose, require the beams to stay symmetric after deformation. We study the equilibrium states of a beam, which can be found by energy minimization. Chapter 2 is an analytical chapter. In this chapter we derive a differential equation and solve the equation for initially straight beams with a moment applied on the endpoints of the beam. In chapter 3 we plot equilibrium branches and beam shapes. In chapter 4 we study stability. In chapter 5 we study beams with a constant pre-curvature. Finally, we are able to answer the question

How far can we push the elastica keeping the model continuous?

Chapter 2

Analytical description of a beam

In this chapter we will set up a model for the description of an one-dimensional beam on which a moment and a force are applied. Using Energy minimization we derive a differential equation and solve it for initially straight beams. Eventually we check whether we find Euler buckling when no moment is applied.

2.1 Elastica

Consider an one-dimensional beam made of elastic material, as sketched in figure 2.1. $\overline{M}$ is the moment applied on the beam and $\overline{P}$ the force. The curvilinear coordinate is given by s and the angle between the beam and the horizontal by $\theta(s)$. α is the angle at $s = 0$ and Δu is the horizontal displacement. A force $\overline{P}$ and a moment $\overline{M}$ are applied at the endpoints of the beam.

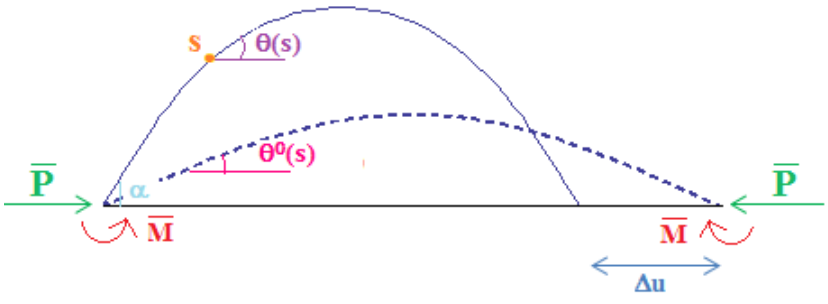

Figure 2.1: *Sketch of a beam, with a moment $\overline{M}$ and a force $\overline{P}$ applied on the endpoints. The solid line is the position of the beam and the dashed line is its initial position.*

We assume that the beam is inextensible and has length l. The left endpoint of the beam is fixed at the origin and the other end of the beam is free to move along the horizontal axis, see figure 2.1. We use the arc length parametrization to denote the position on the beam. This means we describe the length of the beam by the arc length. The length of arc along a curve $\gamma(t)$ from a reference point a is given by $s(t) = \int_a^t |\gamma'(v)|dv$ [7]. Let $u(s)$ be the displacement of the beam in the x-direction and $w(s)$ the displacement in the y-direction. Since $\theta(s)$ is the angle between the tangent at point s and the horizontal line through point s, the curvature κ is given by

$$\kappa = \frac{\partial \theta}{\partial s} =: \theta_s(s). \tag{2.1}$$

The angle between the tangent at point s and the horizontal line trough point s in the initial position of the beam is denoted by θ^0 and the precurvature is denoted by θ_s^0. The applied moment $\overline{M}$ is the bending moment, which is equal to $\overline{M} = EI\kappa$. Where E is Young's modulus, which is given by

$$E = \frac{\text{stress}}{\text{strain}}. \tag{2.2}$$

Stress represents the internal forces that cause deformation within the material and strain describes the resulting deformation.
I is called the second moment of area and is a measure of the ability of a beam to resist bending due to geometry. The product of these two EI is known as the bending stiffness [8]. $\overline{M}$ is defined to be positive when the moment on the left endpoint of the beam is directed clockwise. Otherwise the moment is negative. We do not study the dynamics of buckling and bending but the static equilibrium states of the beam.

2.2 Boundary conditions

We want to specify the angle at the endpoints of the beam and the curvature at the endpoints. Let α be the angle at one endpoint of the beam. Then because of symmetry the angle at the other endpoint of the beam is given by $-\alpha$. The bending moment is applied on the endpoint. Therefore the problem has the following boundary conditions:

$$\begin{aligned} &\theta(0) = \alpha + \theta^0(0),\ \theta(l) = -\alpha + \theta^0(l), \\ &\theta_s(0) = \frac{\overline{M}}{EI} + \theta_s^0(0),\ \theta_s(l) = -\frac{\overline{M}}{EI} + \theta_s^0(l). \end{aligned} \tag{2.3}$$

2.3 Definition of modes

We define the number of arcs to be the number of modes of a beam. Figure 2.2 shows a beam in the third mode. Let $n \in \mathbb{N}$ denote the number of modes. We call $n = 1$ the first mode and $n = 2, 3, 4, ...$ the higher modes. We only consider symmetric beams, therefore n must be odd.

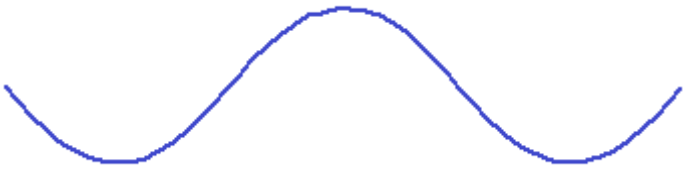

Figure 2.2: *Beam with 3 arcs. So $n = 3$, the beam is in the third mode.*

2.4 Differential equation

2.4.1 Energy

Since we study equilibrium states of the beam, there is no kinetic energy. Because the beam is inextensible the linear energy density of the beam is the bending energy.

$$E_{ben} = \int_0^{\kappa-\kappa_0} \overline{M}(\kappa')d\kappa'. \tag{2.4}$$

Since we want to know the energy of the beam, we have to integrate over the length of the beam. Therefore the elastic energy becomes

$$E_{ben} = \int_0^l ds \int_0^{\kappa-\kappa_0} \overline{M}(\kappa')d\kappa'. \tag{2.5}$$

Substituting $\overline{M} = EI\kappa$ and recalling the curvature $\kappa = \theta_s$, the energy of the beam is

$$E_{ben} = \frac{EI}{2} \int_0^l (\theta_s - \theta_s^0)^2 ds. \tag{2.6}$$

2.4.2 Mechanical equilibrium by energy minimization

Nature requires a system to be in a state of minimal energy. Therefore we can find the equilibrium states by minimizing the energy. We want to minimize the energy under the geometrical constraint of finite Δu, see

figure 2.1. If we do not include the constraint in the minimization, the equilibrium state would be a straight beam. The displacement of the beam Δu is given by the integral over the beam arc length. u_s is the projection of the beam on the x-axis in the initial configuration minus the projection of the beam on the x-axis in the equilibrium state. Therefore

$$\Delta u = \int_0^l \Big(\cos(\theta^0) - \cos(\theta)\Big)\, ds. \tag{2.7}$$

To minimize the elastic energy under the constraint (2.7) we use Lagrange multipliers [9]. Let λ be a Lagrange multiplier. Then the Lagrangian is given by

$$\overline{\Lambda} = E_{el} + \lambda \left(\Delta u - \int_0^l \Big(\cos(\theta^0) - \cos(\theta)\Big)\, ds\right). \tag{2.8}$$

To find the minimal energy under the constraint (2.7) we must have $\delta\overline{\Lambda} = 0$. Therefore

$$\delta\overline{\Lambda} = \frac{\partial\overline{\Lambda}}{\partial\theta_s}\delta\theta_s + \frac{\partial\overline{\Lambda}}{\partial\theta}\delta\theta^0 = \int_0^l \Big(EI\left(\theta_s - \theta_s^0\right)\delta\theta_s - \sin(\theta)\delta\theta\Big)\, ds = 0. \tag{2.9}$$

We use integration by parts $\int_0^l \theta_s\delta\theta_s ds = [\theta_s\delta\theta]_0^l - \int_0^l \theta_{ss} ds$, where $[\theta_s\delta\theta]_0^l = 0$ because $\delta\theta = 0$ at the boundaries.
Also integrating by parts $\theta_{ss}^0\delta\theta$ and substituting both in (2.9) gives

$$\delta\overline{\Lambda} = \int_0^l \Big(EI\left(-\theta_{ss} + \theta_{ss}^0\right)\delta\theta - \lambda\sin(\theta)\delta\theta\Big)\, ds = 0. \tag{2.10}$$

The integral should be zero for arbitrary $\delta\theta$, therefore the integrand is zero. So

$$EI\left(-\theta_{ss} + \theta_{ss}^0\right)\delta\theta - \lambda\sin(\theta)\delta\theta = 0. \tag{2.11}$$

To determine the physical meaning of the Lagrange multiplier λ we take a look at the dimensions
$[E] = [force][length]^{-2}, [I] = [length]^4, [\theta_{ss}] = [\theta_{ss}^0] = [length]^{-2}$. Therefore $\left[EI\left(-\theta_{ss} + \theta_{ss}^0\right)\right] = [force]$, so also $[\lambda] = [force]$. Thus $\lambda = \overline{P}$, the force applied on the endpoints of the beam, required to displace one end by an amount of Δu. So the nonlinear inhomogeneous differential equation describing a beam is

$$\theta_{ss} - \theta_{ss}^0 + \frac{\overline{P}}{EI}\sin(\theta) = 0. \tag{2.12}$$

The nonlinearity comes from $\dfrac{\overline{P}}{EI}\sin(\theta)$ and the inhomogeneity from θ_{ss}^0.

2.5 Nondimensionalization

The unit of s is l. Since we want to work with dimensionless equations we scale s by the length of the beam. Therefore we define $t = \frac{s}{l}$. Then $\theta_{ss} = \frac{1}{l^2}\theta_{tt}$. We introduce the dimensionless force $P = \frac{\overline{P}l^2}{EI}$. As a result the dimensionless differential equation is given by

$$\theta_{tt} - \theta^0_{tt} + P\sin(\theta) = 0. \tag{2.13}$$

Similarly we want to turn the boundary conditions into dimensionless boundary conditions. Therefore we introduce the dimensionless moment $M = \frac{\overline{M}l}{EI}$. Then the boundary conditions become

$$\begin{aligned} &\theta(0) = \alpha + \theta^0(0),\ \theta(1) = -\alpha + \theta^0(1), \\ &\theta_t(0) = M + \theta^0_t(0),\ \theta_t(1) = -M + \theta^0_t(1). \end{aligned} \tag{2.14}$$

Because of the scaling the beam has now length one.

2.6 Solution for beams without pre-curvature

In the former section we derived a nonlinear inhomogeneous differential equation (2.13). For simplicity we consider initially straight beams. For this beams $\theta_0 = 0$. Therefore the differential equation becomes a nonlinear homogeneous equation

$$\theta_{tt} + P\sin(\theta) = 0, \tag{2.15}$$

with the boundary conditions

$$\begin{aligned} &\theta(0) = \alpha,\ \theta(1) = -\alpha, \\ &\theta_t(0) = M,\ \theta_t(1) = -M. \end{aligned} \tag{2.16}$$

2.6.1 First solution

To obtain the first solution we follow the approach of W. Schouten [10]. To solve this equation note that it is the same equation as the equation of a nonlinear pendulum [11]. First we multiply with θ_t. This gives

$$\theta_t\left(\theta_{tt} + P\sin(\theta)\right) = 0, \tag{2.17}$$

which we write as

$$\frac{d}{dt}\left(\frac{1}{2}\theta_t^2 - P\cos(\theta)\right) = 0. \tag{2.18}$$

Integration gives

$$\frac{1}{2}\theta_t^2 - P\cos(\theta) = c, \tag{2.19}$$

with c $\in \mathbb{R}$ an arbitrary constant. Using the boundary conditions we find

$$\theta_t^2 = M^2 - 2P\cos(\alpha) + 2P\cos(\theta). \tag{2.20}$$

To rewrite this equation we use the trigonometric formula $\cos(\theta) = \left(1 - 2\sin^2\left(\frac{\theta}{2}\right)\right)$, this gives

$$\theta_t^2 = 4P\left(\frac{1}{2}\left(\frac{M^2}{2} - \cos(\alpha) + 1\right) - \sin^2\left(\frac{\theta}{2}\right)\right). \tag{2.21}$$

Let $k = \frac{1}{2}\left(\frac{M^2}{2P} - \cos(\alpha) + 1\right)$ and substitute $\tau = \sqrt{P}t$ and $z = \frac{y}{\sqrt{k}}$.
Note that this substitution gives periodic solutions. Therefore the solution is only valid for $-\pi < \alpha < \pi$. Then the equation becomes

$$\left(\frac{dz}{d\tau}\right)^2 = (1 - z^2)(1 - kz^2). \tag{2.22}$$

Separation of variables gives

$$d\tau = \pm\frac{dz}{\sqrt{(1 - z^2)(1 - kz^2)}}. \tag{2.23}$$

From the boundary condition $\theta(0) = \alpha$ follows $z(0) = \frac{y(0)}{\sqrt{k}} = \frac{\sin\left(\frac{\alpha}{2}\right)}{\sqrt{k}}$.
We will use this to solve (2.23). Integrating gives

$$\tau + \tilde{c} = \pm\int_{\frac{\sin\left(\frac{\alpha}{2}\right)}{\sqrt{k}}}^{z} \frac{dz}{\sqrt{(1 - z^2)(1 - kz^2)}}, \tag{2.24}$$

with $\tilde{c}$ an arbitrary constant. This step is only valid for monotonic θ.
Note that when $z = \frac{\sin\left(\frac{\alpha}{2}\right)}{\sqrt{k}}$,

$$\tau(0) + \tilde{c} = 0. \tag{2.25}$$

Because $\tau(0) = 0$ we get

$$\tau = \pm \int_{\frac{\sin\left(\frac{\alpha}{2}\right)}{\sqrt{k}}}^{z} \frac{dz'}{\sqrt{(1-z'^2)(1-kz'^2)}}. \tag{2.26}$$

To eliminate the plus-minus sign we define

$$\text{Sign}(M) := \begin{cases} 1, & M > 0 \\ -1 & M \leq 0 \end{cases} \tag{2.27}$$

and note that $\text{Sign}(M) = \text{Sign}(\theta_t(0)) = \text{Sign}\left(\frac{dz'}{d\tau}\right)$.
Therefore (2.26) can be written as

$$\text{Sign}(M)\tau = \int_{\frac{\sin\left(\frac{\alpha}{2}\right)}{\sqrt{k}}}^{z} \frac{dz'}{\sqrt{(1-z'^2)(1-kz'^2)}}. \tag{2.28}$$

The incomplete elliptic integral of the first kind is defined as [12]

$$F(x;k) = \int_0^x \frac{dz}{\sqrt{(1-z^2)(1-k^2z^2)}}. \tag{2.29}$$

To use this expression we have to rewrite (2.28) to an integral starting at zero. Therefore we calculate the integral from zero to z and subtracting the integral from zero to $\frac{\sin\left(\frac{\alpha}{2}\right)}{\sqrt{k}}$, which results in

$$\text{Sign}(M)\tau = F(z;\sqrt{k}) - F\left(\frac{\sin\left(\frac{\alpha}{2}\right)}{\sqrt{k}};\sqrt{k}\right). \tag{2.30}$$

As we want to have an explicit solution of θ we write

$$F(z;\sqrt{k}) = \text{Sign}(M)\tau + F\left(\frac{\sin\left(\frac{\alpha}{2}\right)}{\sqrt{k}};\sqrt{k}\right) \tag{2.31}$$

and use that for $F(x;k) = u$, the Jacobian elliptic function is given by $sn(u;k) = x$ [12].
Therefore we obtain

$$sn\left(F\left(\frac{\sin\left(\frac{\alpha}{2}\right)}{\sqrt{k}};\sqrt{k}\right) + \text{Sign}(M)\tau;\sqrt{k}\right) = \frac{\sin\left(\frac{\theta}{2}\right)}{\sqrt{k}}. \tag{2.32}$$

Inverting this equation gives

$$\theta = 2\sqrt{k}\arcsin\left(sn\left(F\left(\frac{\sin\left(\frac{\alpha}{2}\right)}{\sqrt{k}};\sqrt{k}\right)+\text{Sign}(M)\sqrt{P}t;\sqrt{k}\right)\right), \quad (2.33)$$

with $k = \frac{1}{2}\left(\frac{M^2}{2P} - \cos(\alpha) + 1\right) = \frac{M^2}{4P} + \sin^2\left(\frac{\alpha}{2}\right)$.

θ is a function of four parameters: M,P, α and t. Given the beam stays symmetric after deformation we can use $\theta = 0$ at $t = \frac{1}{2}$ to reduce the number of parameters from five to three. This results in an implicit equation of M, P and α, namely

$$2\sqrt{k}\arcsin\left(sn\left(F\left(\frac{\sin\left(\frac{\alpha}{2}\right)}{\sqrt{k}};\sqrt{k}\right)+\text{Sign}(M)\sqrt{P}\frac{1}{2};\sqrt{k}\right)\right) = 0, \quad (2.34)$$

with $k = \frac{M^2}{4P} + \sin^2\left(\frac{\alpha}{2}\right)$.
Because $\sqrt{k} \neq 0$ we can write equation (2.34) as

$$sn\left(F\left(\frac{\sin\left(\frac{\alpha}{2}\right)}{\sqrt{k}};\sqrt{k}\right)+\text{Sign}(M)\sqrt{P}\frac{1}{2};\sqrt{k}\right) = 0. \quad (2.35)$$

This equation provides solutions for monotonic θ and non-monotonic θ, as we will see in chapter 3. Equation (2.35) can be written as

$$\text{Sign}(M)\frac{1}{2}\sqrt{P} + F\left(\frac{\sin\left(\frac{\alpha}{2}\right)}{\sqrt{k}};\sqrt{k}\right) = 2nK(k), \quad (2.36)$$

with $n = 0, 1, 2, ...$ [12]. The solution for $n = 0$ corresponds to monotonic θ and the solutions for $n = 1, 2, 3, ...$ correspond to non-monotonic θ, as we will see in chapter 3. The derivation of this solution is only valid for monotonic θ, because taking the integral from $z(0)$ to z is only allowed for monotonic θ. In section 2.6.3 we will see that the solutions for non-monotonic θ probably also give the correct results.

2.6.2 Second solution

We distinguish the cases θ is monotonic and θ is non-monotonic. For a beam in the first mode θ is monotonic for $M > 0$ and $\alpha < 0$, θ is negative

at $t = 0$ and increases until $\theta = 0$ at $t = \frac{1}{2}$. θ is also monotonic for $M < 0$ and $\alpha > 0$, θ is positive at $t = 0$ and decreases until $\theta = 0$ at $t = \frac{1}{2}$. When $M > 0$ then the curvature at $t = 0$ is positive $\theta_t(0) > 0$. This means that for α positive θ first must increase and θ will also decrease because it is zero at $t = \frac{1}{2}$. Therefore θ is non-monotonic for $M > 0$ and $\alpha > 0$. Similarly can be derived that θ is non-monotonic for $M < 0$ and $\alpha < 0$.

First we consider monotonic θ. From equation (2.20) we know that we can write θ_t as

$$\theta_t = \pm\sqrt{M^2 - P\cos(\alpha) + 2P\left(1 - 2\sin^2\left(\frac{\theta}{2}\right)\right)}. \tag{2.37}$$

Take $C = 2P(1 - \cos(\alpha)) + M^2$ and use separation of variables to write

$$dt = \text{Sign}(M)\frac{d\theta}{\sqrt{C}\sqrt{1 - \frac{4P}{C}\sin^2\left(\frac{\theta}{2}\right)}}. \tag{2.38}$$

Given the beam stays symmetric after deformation and the fact that θ is monotonic, we can integrate equation (2.38) as follows,

$$\int_0^1 dt = \text{Sign}(M)\frac{2}{\sqrt{C}}\int_\alpha^0 \frac{d\theta}{\sqrt{1 - \frac{4P}{C}\sin^2\left(\frac{\theta}{2}\right)}}. \tag{2.39}$$

Substitution of $y = \dfrac{\theta}{2}$ gives

$$1 = -\text{Sign}(M)\frac{4}{\sqrt{C}}\int_0^{\frac{\alpha}{2}} \frac{dy}{\sqrt{1 - \frac{4P}{c}\sin^2(y)}}. \tag{2.40}$$

Using the definition of the incomplete elliptic integral of the first kind [12], the solution becomes

$$1 = -\text{Sign}(M)\frac{4}{\sqrt{C}}F\left(\frac{\alpha}{2}; \frac{4P}{C}\right), \tag{2.41}$$

with $C = 2P(1 - \cos(\alpha)) + M^2$.

Now we obtain an expression for θ. Take $\theta > 0$ and $t < \frac{1}{2}$. Note that for monotonic θ and $\theta > 0$ and $t < \frac{1}{2}$, M must be negative. Then integrating equation (2.37) gives

$$t = \frac{\text{Sign}(M)}{\sqrt{C}} \int_{\alpha}^{\theta} \frac{dt}{\sqrt{1 - \frac{4P}{C}\sin^2\left(\frac{\theta}{2}\right)}}. \tag{2.42}$$

Substitution of $y = \dfrac{\theta}{2}$ and then splitsing the integral in an integral from zero to $\dfrac{\theta}{2}$ minus an integral from zero to $\dfrac{\alpha}{2}$ gives

$$t = -\frac{1}{\sqrt{C}}\left(F\left(\frac{\theta}{2}; \frac{4P}{C}\right) - F\left(\frac{\alpha}{2}; \frac{4P}{c}\right)\right), \tag{2.43}$$

with $C = 2P(1 - \cos(\alpha)) + M^2$. In a similar way the solutions for $M < 0$, $t > \dfrac{1}{2}$ and for $M > 0, t > \dfrac{1}{2}$ and for $M > 0$, $t < \dfrac{1}{2}$. can be obtained.

Now we consider non-monotonic beams. Assume that the beam is in the first mode and $\theta(0) = \alpha > 0$ and $\theta_t(0) = M > 0$. Note that for these conditions θ is non-monotonic. Therefore in $\theta_t > 0$ in the beginning and then $\theta_t < 0$. According to the mean value theorem [13] there exists a point θ_t* between $t = 0$ and $t = \dfrac{1}{2}$ for which $\theta_t = 0$. We use again that θ can be written as (2.20), also using trigonometrical formulas we obtain

$$\theta_t^2 = M^2 + 4P\left(\sin^2\left(\frac{\alpha}{2}\right) - \sin^2\left(\frac{\theta}{2}\right)\right). \tag{2.44}$$

Thus $\theta_t = 0$ for

$$\sin\left(\frac{\theta*}{2}\right) = \sqrt{\sin^2\left(\frac{\alpha}{2}\right) + \frac{M^2}{4P}}, \tag{2.45}$$

under the condition that $\sin^2\left(\dfrac{\alpha}{2}\right) + \dfrac{M^2}{4P} \leq 1$ and $\alpha < \theta < \dfrac{\pi}{2}$.
Then $\theta*$ is given by $\theta* = \arcsin\left(\sqrt{\sin^2\left(\frac{\alpha}{2}\right) + \frac{M^2}{4P}}\right)$. To integrate we have to split the beam in four parts, as shown in figure 2.3. In each part θ is monotonic. We have to integrate equation (2.38) for each part sepeartely, because limits of integration are different.

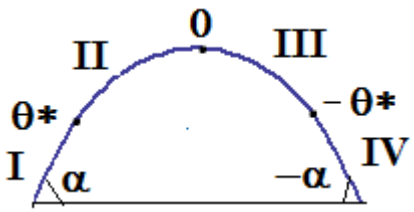

Figure 2.3: *Schematic sketch of a beam in the first mode, which is divided in four parts. The parts should be integrated separately.*

Let t_1 be the position of $\theta*$. For part I we obtain from (2.38) the following expression

$$\int_0^{t_1} dt = \int_\alpha^{\theta*} \frac{d\theta}{\sqrt{C}\sqrt{1 - \frac{4P}{C}\sin^2\left(\frac{\theta}{2}\right)}}. \tag{2.46}$$

Substitution of $y = \sin\left(\frac{\theta}{2}\right)$ gives

$$t_1 = \frac{2}{\sqrt{C}} \int_{\frac{\alpha}{2}}^{\frac{\theta*}{2}} \frac{dy}{\sqrt{1 - \frac{4P}{c}\sin^2(y)}}. \tag{2.47}$$

With the use of the definition of the incomplete elliptic integral of the first kind [12] the solution becomes

$$t_1 = \frac{2}{\sqrt{C}}\left(F\left(\frac{\theta*}{2}; \frac{4P}{C}\right) - F\left(\frac{\alpha}{2}; \frac{4P}{C}\right)\right), \tag{2.48}$$

with $C = 2P(1 - \cos(\alpha)) + M^2$ and $\theta* = \arcsin\left(\sqrt{\sin^2\left(\frac{\alpha}{2}\right) + \frac{M^2}{4P}}\right)$.

The other parts can be integrated in a similar way. For part II we have to integrate from $\theta*$ to 0, this gives

$$\frac{2}{\sqrt{C}} F\left(\frac{\theta*}{2}; \frac{4P}{C}\right). \tag{2.49}$$

For part III we have to integrate from 0 to $-\theta*$, which results in

$$\frac{2}{\sqrt{C}} F\left(\frac{\theta*}{2}; \frac{4P}{C}\right). \tag{2.50}$$

Finally, for part IV the integral goes from $-\theta*$ to $-\alpha$, which leads to

$$\frac{2}{\sqrt{C}}\left(F\left(\frac{\theta*}{2}; \frac{4P}{C}\right) - F\left(\frac{\alpha}{2}; \frac{4P}{C}\right)\right). \tag{2.51}$$

So the solution is given by the sum over the four parts, which results in

$$\frac{2}{\sqrt{C}}\left(4F\left(\frac{\theta*}{2};\frac{4P}{C}\right)-2F\left(\frac{\alpha}{2};\frac{4P}{C}\right)\right)=1. \tag{2.52}$$

For $M>0$, $\alpha<0$ and $n=3$ we obtain the same solution, the beam consists of three arcs with monotonic θ.
The calculation goes similar for higher modes, only the beam must be divided in more parts. For three arcs with non-monotonic θ the beam must be divided in eight parts, as shown in figure 2.4.

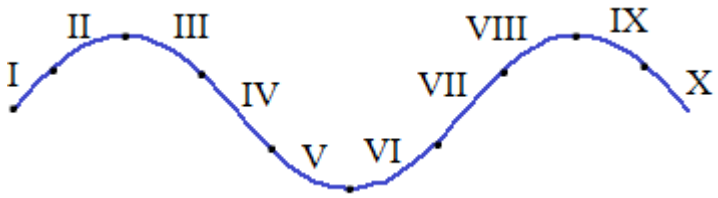

Figure 2.4: *Schematic sketch of a beam in the third mode, which is divided in 10 parts.The parts should be integrated separately.*

For most parts the solution can be obtained in the way the solution for the parts of the beam in the first mode are obtained. However the integral for part IV and VII are zero because in part IV the integration limits are both $-\theta*$ and in part VII the integration limits are both $\theta*$. Then the solution is given by

$$\frac{2}{\sqrt{C}}\left(8F\left(\frac{\theta*}{2};\frac{4P}{C}\right)-2F\left(\frac{\alpha}{2};\frac{4P}{C}\right)\right)=1, \tag{2.53}$$

with $C=2P(1-\cos(\alpha))+M^2$ and $\theta*=\arcsin\left(\sqrt{\sin^2\left(\frac{\alpha}{2}\right)+\frac{M^2}{4P}}\right)$. A beam with five arcs with monotonic θ has the same solution. This method can be extended for the other higher modes. A general solution is given by

$$\frac{2}{\sqrt{C}}\left((2n+2)F\left(\frac{\theta*}{2};\frac{4P}{C}\right)-2F\left(\frac{\alpha}{2};\frac{4P}{C}\right)\right)=1, \tag{2.54}$$

with $C=2P(1-\cos(\alpha))+M^2$ and $\theta*=\arcsin\left(\sqrt{\sin^2\left(\frac{\alpha}{2}\right)+\frac{M^2}{4P}}\right)$. This solution is valid for both monotonic and non-monotonic θ.
An expression for θ must also be calculated separately for each part. For each part the solution can be obtained in a similar way as for beams with monotonic θ.

2.6.3 Hypothesis

We suspect that both solutions give the same results for both monotonic and non-monotonic θ. At a late stage of this project we found out that the derivation of the solution obtained by W. Schouten [10] is methodologically incorrect for non-monotonic θ. Within our time limit we could derive a second solution. Then we plotted both solutions up to and including the to the third mode in one figure. The lines coincide. Therefore we suspect the solutions to give the same results for all modes. To be certain, a transformation to rewrite one solution as the other needs to be found.

2.7 Euler buckling

For $M = 0$, the problem of an elastic beam is well defined. Euler discovered that if a force is applied to a beam, first the straight beam is stable and at a critical force $P \approx \pi^2$, the straight beam becomes unstable and the beam buckles with equal probability into one of the two directions. This is caused by a pitchfork bifurcation, see figure 2.5. This buckling behaviour is called Euler buckling [2].

2.7.1 Euler buckling for the first solution

For $M = 0$, θ is monotonic so we have to take $n = 0$ in equation (2.36). Substituting $M = 0$ gives

$$1 = \frac{2}{\sqrt{P}} K\left(\sin^2\left(\frac{\alpha}{2}\right)\right), \tag{2.55}$$

with $K(k) = F\left(1; \sqrt{k}\right)$ the complete elliptic integral of the first kind. Now we assume the deflections to be small, so $\alpha << 1$. Then we can perform a Taylor expansion of $\sin^2\left(\frac{\alpha}{2}\right)$ around $\alpha = 0$. This gives

$$\sin^2\left(\frac{\alpha}{2}\right) \approx \frac{\alpha^2}{4} + O(\alpha^4). \tag{2.56}$$

The Taylor expansion for $K(k)$ around $k = 0$ is given by [12]

$$K(k) \approx \frac{\pi}{2}\left(1 + \frac{1}{4}\frac{k}{1-k} + \frac{1}{8}\frac{k^2}{1-k^2}\right) + O(k^3). \tag{2.57}$$

Therefore equation (2.55) can be written as

$$K\left(\frac{\alpha^2}{2}\right) \approx \frac{\pi}{2}\left(1 + \frac{1}{4}\frac{\alpha^2}{4-\alpha^2}\right) + O(\alpha^4). \tag{2.58}$$

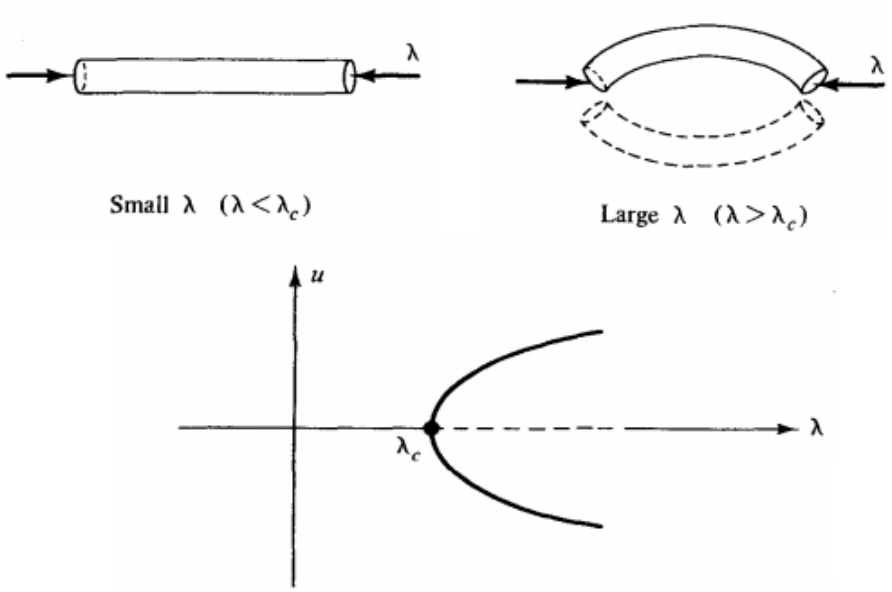

Figure 2.5: *Euler buckling. λ corresponds to P, the force applied on the endpoints of the beam and $\lambda_c = P_c$, the critical buckling force. u corresponds to α. The beam is straight for $\lambda < \lambda_c$ and above the critical force the beam buckles with equal probability into one of the two directions. The (u, λ)-diagram shows the corresponding pitchfork bifurcation. [2].*

Then using again a Taylor expansion around $\alpha = 0$ we get

$$\frac{\alpha^2}{2 - \alpha^2} \approx \frac{\alpha^2}{16} + O(\alpha^4). \tag{2.59}$$

Thus we find an explicit equation of P expressed in α given by

$$P \approx \pi^2 \left(1 + \frac{\alpha^2}{16}\right)^2 \approx \pi^2 \left(1 + \frac{\alpha^2}{8}\right) + O(\alpha^4). \tag{2.60}$$

So we see that below a critical force $P_c \approx \pi^2$ the zero solution is stable and for $P > P_c$ the beam buckles. The beam buckles either into the upper half plane , positive α, or into the lower half plane, negative α. So at the buckling point $P = P_c$ we see a pitchfork bifurcation, see figure 2.6. So for $M = 0$ we find Euler buckling, this confirms that the solution is correct for monotonic θ.

2.7.2 Euler buckling for the second solution

To verify that the second solution is also correct for monotonic θ we have to find Euler for $M = 0$. The equation for monotonic θ which is given by

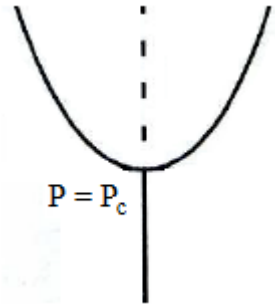

Figure 2.6: *Pitchfork bifurcation at $P = P_c$.*

(2.41). Substitution of $M = 0$ gives

$$\sqrt{C} = 4F\left(\frac{\alpha}{2}; \frac{4P}{C}\right), \tag{2.61}$$

with $C = 4P\sin^2\left(\frac{\alpha}{2}\right)$. Equation (2.61) can be written as

$$\sqrt{C} = 4F\left(\frac{\alpha}{2}; \frac{1}{\sin^2\left(\frac{\alpha}{2}\right)}\right). \tag{2.62}$$

Take $m = \dfrac{1}{\sin^2\left(\frac{\alpha}{2}\right)}$, then $\text{arccosecant}(\sqrt{m}) = \dfrac{\alpha}{2}$. Therefore (2.62) can be written as

$$\sqrt{C} = 4F\left(\text{arccosecant}(\sqrt{m}), m\right). \tag{2.63}$$

To rewrite this equation we will use transformations for fixed m [14], namely

$$F\left(\text{arccosecant}(\sqrt{m}); m\right) = \frac{1}{\sqrt{m}}K\left(\frac{1}{m}\right). \tag{2.64}$$

Equation (2.63) can be written as

$$\sqrt{C} = \frac{4}{\sqrt{m}}K\left(\frac{1}{m}\right). \tag{2.65}$$

Note that $\sqrt{C} = 2\sqrt{P}\left|sin\left(\frac{\alpha}{2}\right)\right|$. Substituting back $m = \dfrac{1}{\sin^2\left(\frac{\alpha}{2}\right)}$ gives

$$2K\left(\sin^2\left(\frac{\alpha}{2}\right)\right) = \sqrt{P}\frac{|\sin\left(\frac{\alpha}{2}\right)|}{\sin\left(\frac{\alpha}{2}\right)}, \tag{2.66}$$

which can be written as

$$\text{sign}(\alpha)\sqrt{P} = 2K\left(\sin^2\left(\frac{\alpha}{2}\right)\right). \tag{2.67}$$

Therefore we obtain the same equation as for solution one, equation (2.55). Thus also for this solution we find Euler buckling. Concluding, both solutions are correct for monotonic θ.

Chapter 3

Equilibrium branches

The implicit equations obtained in section 2.6 cannot be solved analytically. Therefore we will use Mathematica to plot the solutions. We want to explore the relation between the moment M, the force P and the angle at the endpoints of the beam α. As explained in section 2.6.1 we can use the symmetry of the beam to obtain an implicit equation of P, M and α, equation (2.35). From this equation we can plot the equilibrium branches in the (P, α)-, (M, α)-diagrams and the 3D-plot. Due to a lack of time we did not use the second solution in the analyses of the equilibrium branches.

3.1 Determining beam shapes

We can deduce the shape of the beam from its deflection. As we have seen in section 2.4.2 the displacement of the beam in the x-direction is given by $\Delta u = \int_0^1 \Big(cos(\theta^0) - \cos(\theta)\Big)\, dt$. Therefore the displacement of each point of the beam along the horizontal axis can be calculated by $u(t) = \int_0^t \Big(\cos(\theta^0) - \cos(\theta)\Big)\, dt'$. Similarly the displacement of each point on the beam in the y-direction is given by $w(t) = \int_0^t \Big(\sin(\theta) - \sin(\theta^0)\Big)\, dt'$. To determine the values u and w, we numerically calculate the value of the integral for several values of t. For this we need to know the values of P, M and α, which can be determined numerically, using equation (2.35). Let $x^0(t)$, $y^0(t)$ be the initial positions of the beam. Then the position of the

beam is described by

$$\begin{aligned} x(t) &= x^0(t) + u(t), \\ y(t) &= y^0(t) + w(t). \end{aligned} \tag{3.1}$$

Because our beam has no pre-curvature the initial position of the beam is given by $x^0(t) = t$ and $y^0(t) = 0, \forall t$. So the beam shape is given by

$$\begin{aligned} x(t) &= t + u(t), \\ y(t) &= w(t). \end{aligned} \tag{3.2}$$

3.2 (P, α)-diagram

In section 2.7 we already found Euler buckling for $M = 0$, with the corresponding pitchfork bifurcation at $P = P_c$. Now we will explore what happens when we take M finite but small.

3.2.1 (P, α)-diagram for monotonic θ

To get more insight in the physical meaning of a monotonic θ, we first study the (P, α)-diagram for monotonic θ. Figure 3.1 shows a plot of the (P, α)-diagram for several values of M. For $M = 0$ the diagram is symmetric, $\alpha = 0$ for $P < P_c$ and $\alpha \neq 0$ for $P > P_c$. This means that for $P < P_c$ the beam is straight and at $P = P_c$ the beam buckles. From Euler buckling we know the beam buckles with equal probability into the low or upper half plane [15]. Define $P_{Euler}(\alpha)$ as the value of P along the branches that correspond to a buckled beam, the dark green branches in figure 3.1. When we apply a moment the left-right symmetry breaks and buckling is destroyed. This can be seen by the fact that for $M \neq 0$, $\alpha \neq 0$. The beam bends at any value of P and buckling disappears. For positive M the beam bends into the lower half plane and for negative M the beam bends into the upper half plane. The more M departs from zero, the more the beam deflects. This can be seen in figure 3.2 where we take a fixed value of P and plot beam shapes for several values of M. For $P = 2$ the beam corresponding to $M = 0$ is straight.

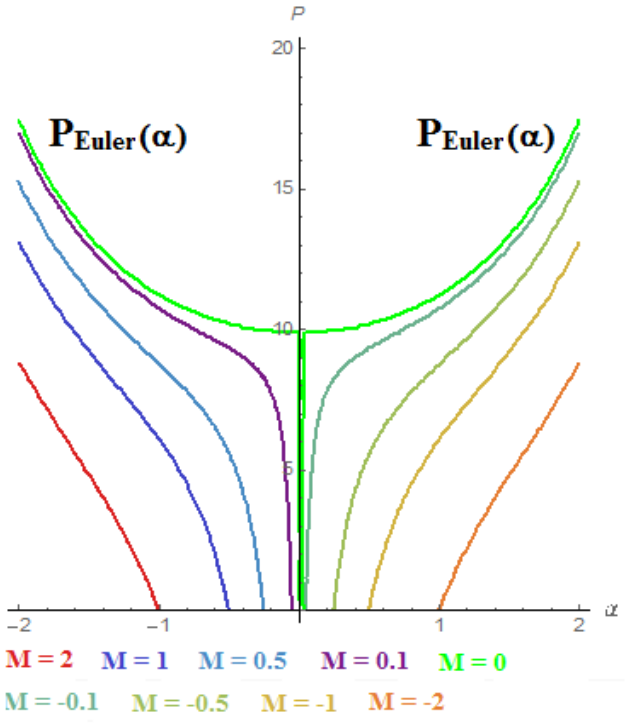

(P, α)-diagram for monotonic θ. The unstable branch of the pitchfork bifurcation is not shown.

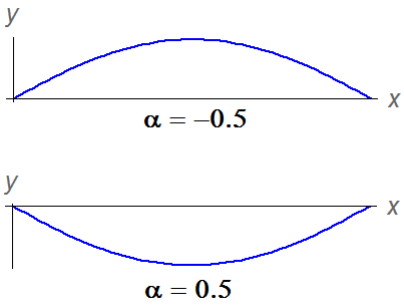

Beam shapes for $M = 0$.

Figure 3.1: *(P, α)-diagram and beam shapes for monotonic θ. The pitchfork occurs for $M = 0$ and the beam buckles for $P > P_c$. The branches that correspond to a buckled beam are called $P_{Euler}(\alpha)$. Applying a moment breaks the symmetry.*

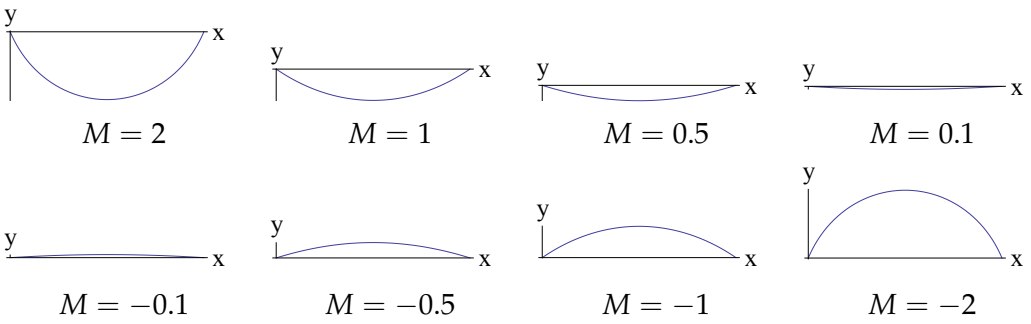

Figure 3.2: *Beam shapes for $P = 2$ and monotonic θ. For $M \neq 0$ the symmetry breaks and the beam bends. The more the moment departs from zero the more the beam deflects.*

3.2.2 Unfolding pitchfork bifurcation

For monotonic θ there are no branches for $M \neq 0$ and $P > P_{Euler}(\alpha)$, see figure 3.1. Since there is a pitchfork bifurcation for $M = 0$ at $P = P_c$, we expect branches for $M \neq 0$ and $P > P_{Euler}(\alpha)$. Figure 3.3 shows the (P, α)-diagram in the case that θ is monotonic and non-monotonic. For $M = 0$ the pitchfork bifurcation is still present and for $M \neq 0$ the pitchfork bifurcation unfolds. For M close to zero the branches are near the branches for $M = 0$. If M departs more from zero the pitchfork bifurcation is further unfolded. Applying a moment gives a preference for a bending direction. The bending direction depends on the sign of the moment. For larger forces above $P_{Euler}(\alpha)$ the deflection of the beam is non-monotonic and the beam switches orientation. This can be seen in figure 3.4.

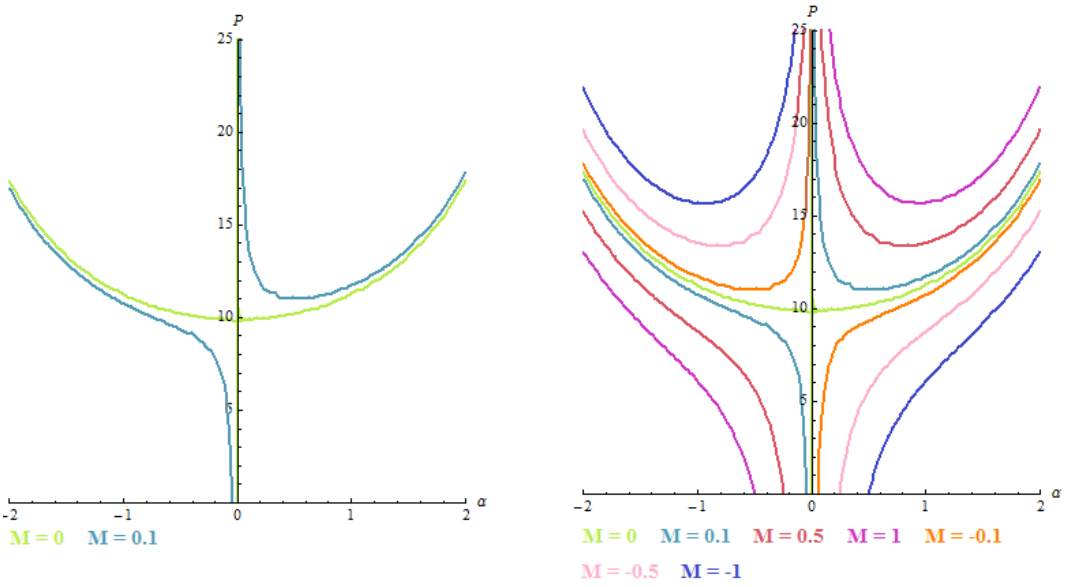

Figure 3.3: *Unfolding pitchfork bifurcation in the (P, α)-diagram for different values of M. The more M departs from zero the further the pitchfork bifurcation is unfolded.*

Figure 3.4: *Beam shapes for $M = 0.1$. The beam shape on left corresponds to $P < P_{Euler}(\alpha)$ and the beam shape on the right to $P > P_{Euler}(\alpha)$. For $P > P_{Euler}(\alpha)$ the beam's deflection is non-monotonic.*

3.2.3 (P, α)-diagram for higher forces

Until now we only considered forces around P_c. From Euler buckling we know that for a symmetric beam each time a pitchfork bifurcation occurs at all $P = n^2\pi^2$ with $n = 1, 3, 5, ...$ [15]. There are no pitchfork bifurcations at even values of n, because we study beams that stay symmetric after deformation. Because of the presence of multiple pitchfork bifurcations, we expect these pitchforks bifurcations to unfold. Figure 3.5 shows the unfolding of the second pitchfork bifurcation at $P = 9P_c$ for several values of M. All lines cross the P-axis but not at the same point.

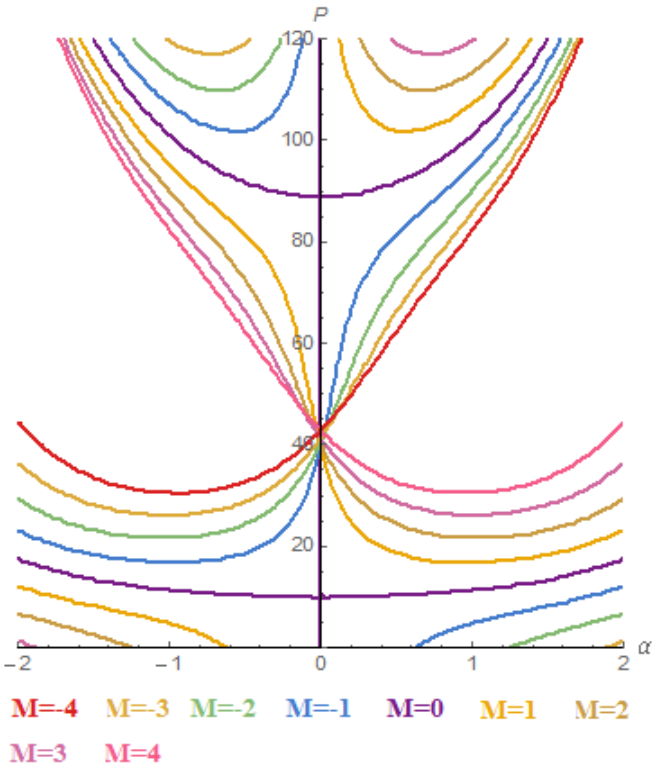

Figure 3.5: *(P, α)-diagram for different values of M, with two unfolding pitchfork bifurcations. The lines cross the $\alpha = 0$-axis at different values of P.*

Figure 3.6 shows the equilibrium branches for one value of M up to and including the third unfolding. P is rescaled by P_c and therefore the unfolding pitchfork bifurcations now take place at $P = (2n+1)^2$, $n \in \mathbb{N}$. Figures 3.7, 3.8, 3.9 and 3.10 show the beam shapes corresponding to the points in figure 3.6. We will follow the branches and explain how the beam shape changes.

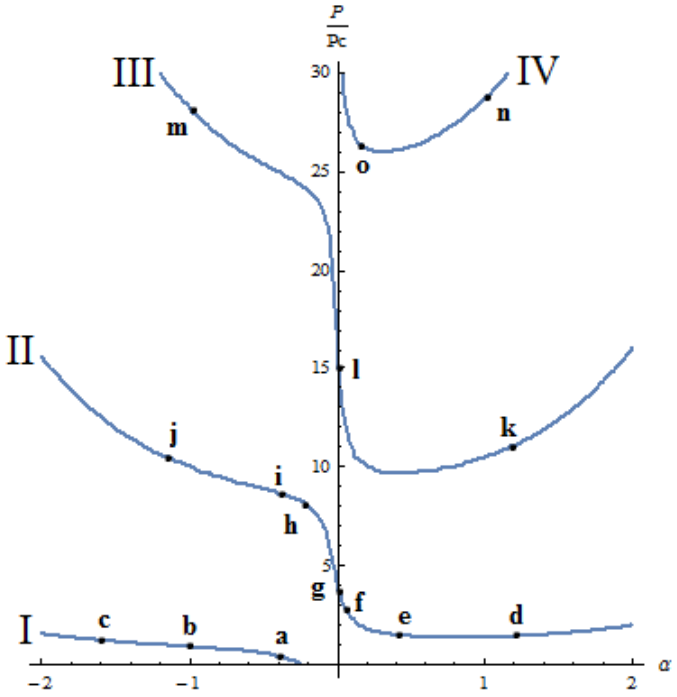

Figure 3.6: *(P, α)-diagram of equilibrium branches for $M = 0.5$, including three unfolded pitchfork bifurcations. The points on branch I, II, III and IV correspond to the beam shapes in figure 3.7, 3.8, 3.9 and 3.10 respectively.*

Branch I lies totally below $P_{Euler}(\alpha)$, the beam is located in the lower half plane and θ is monotonic for these beam shapes. Following this branch from α close to zero to smaller α the deflection of the beam becomes larger. This is shown by beam shapes in figure 3.7.

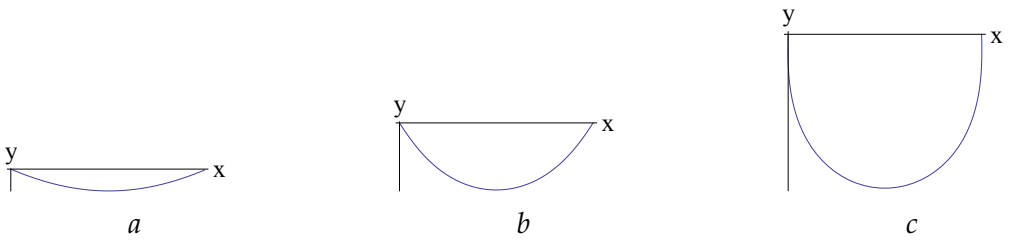

Figure 3.7: *Beam shapes corresponding to the points on branch I in figure 3.6. The deflections is larger for smaller α. θ is monotonic.*

Branch II lies above $P_{Euler}(\alpha)$ and for positive α the beam is located in the upper half plane, see beam shapes d, e and f in figure 3.8. The beam shape is non-monotonic and the orientation of the beam has switched relative to the beams of branch I. When we follow the branch from large α and decrease α we see that first the deflection of the beam becomes smaller until $\alpha = 0$, see beam shapes d, e and f in figure 3.8. At $\alpha = 0$ the deflection is the smallest but not zero, see beam shape g in figure 3.8. If we decrease α further the beams deforms in the third mode and again a smaller α gives a larger deflection, see beam shapes h, i and j in figure 3.8.

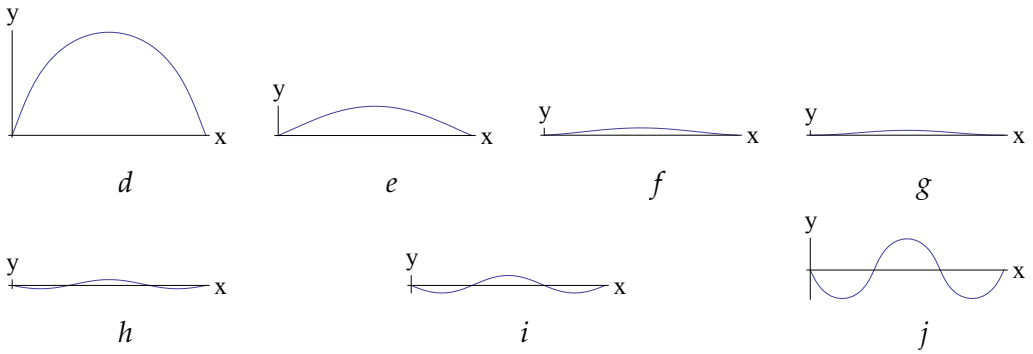

Figure 3.8: *Beam shapes corresponding to the points on branch II in figure 3.6. The more α departs from zero the larger the deflection of the beam. At $\alpha = 0$ the beam is still bent, beam shape g. Beam shapes g, h, i and j show beams in the third mode.*

Now we follow Branch III. The beam is for positive α still in the third mode, see beam shape k in figure 3.9. However the beam has switched orientation relative to the beams for $\alpha < 0$ in branch II, see beam shapes g, h, i and j in figure 3.8. Beam shape l in figure 3.9 shows that also for branch II the beam is not straight for $\alpha = 0$. After crossing the $\alpha = 0$-axis the beam deforms into the fifth mode, see beam shape m in figure 3.9.

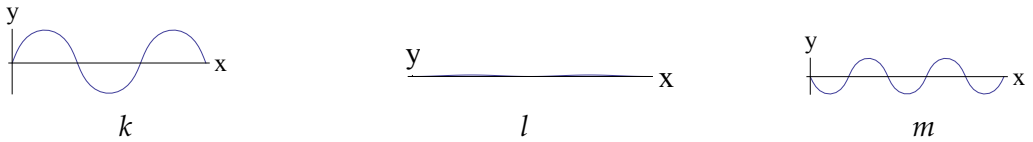

Figure 3.9: *Beam shapes corresponding to the points on branch III in figure 3.6. Beam shape l corresponds to $\alpha = 0$, the beam is bent. Beam shapes k is in the third mode, but has a different orientation than beam shapes g, h, i and j in figure 3.8. Beam shape m is in the fifth mode.*

The beams at branch IV are in the fifth mode, see figure 3.10. The beams have a switched orientation relative to the beams for $\alpha < 0$ of branch III, see beam shape in figure 3.10.

n *o*

Figure 3.10: *Beam shapes corresponding to the points on branch IV in figure 3.6. The beams are in the third mode, but have a different orientation than beam shape k in figure 3.9.*

In general, the more α departs from zero the larger the deflection of the beam and for $M \neq 0$ and $\alpha \neq 0$ the beam is not straight anymore. Each time the $\alpha = 0$-axis is crossed the beam deforms into the next mode and at zero force the beam is bent. If we increase the force, the beam switches orientation and if we increase the force more the beam gets into the next mode and then the same process takes place over and over again.

3.3 (M, α)-diagram

We study the relation between the moment exerted on the endpoints of the beam and the angle at the endpoints of the beam for a fixed value of P.

3.3.1 (M, α)-diagram for monotonic θ

To get more insight in the physical meaning of monotonic θ, we first consider the diagram for monotonic θ. Figure 3.11 shows the relation between M and α for several values of P. For $P < P_c$ the branches in the (M, α)-diagram are monotonic. For $P > P_c$ it seems that the parts for $M > 0$, $\alpha > 0$ and for $M < 0$, $\alpha < 0$ are missing. If $M > 0$ the curvature at $t = 0$ is positive $\theta_t(0) > 0$. This means that for α positive θ first must increase and θ will also decrease because it is zero at $t = \frac{1}{2}$. Therefore θ is non-monotonic for $M > 0$ and $\alpha > 0$. Similarly can be derived that θ is non-monotonic for $M < 0$ and $\alpha < 0$. So the parts that seem to be missing in figure 3.11 correspond to non-monotonic θ.

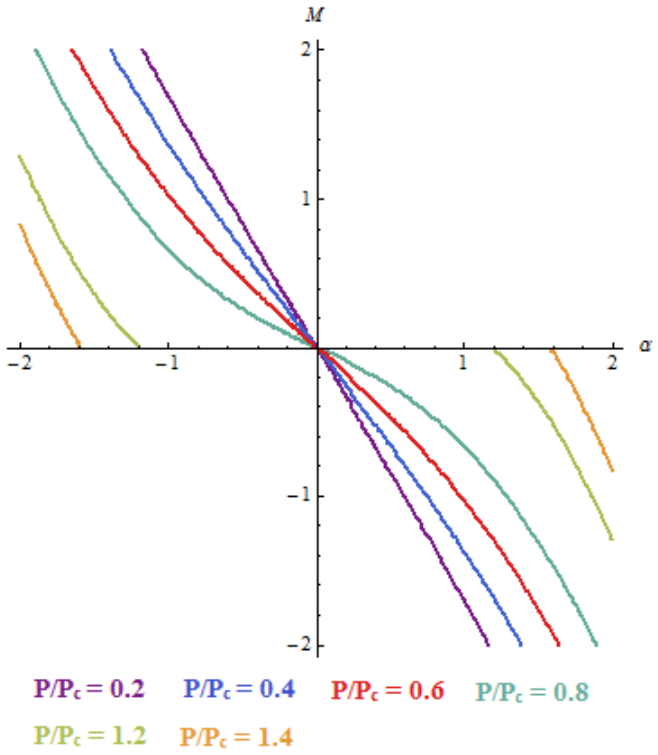

Figure 3.11: *M versus α for monotonic θ. The missing parts of branches corresponding to $P > P_c$ for $M > 0, \alpha > 0$ and for $M < 0, \alpha < 0$ belong to non-monotonic θ.*

3.3.2 Monotonic and non-monotonic θ.

Figure 3.12 shows the relation between M and α in the case where θ can be both monotonic and non-monotonic. Now there are no missing parts, so this confirms that the missing parts correspond to non-monotonic θ. For low P the equilibrium branches in the (M, α)-diagram are almost linear. When P is increased the branches become less linear. For $P < P_c$ the equilibrium branches are monotonic and for $P > P_c$ the equilibrium branches are non-monotonic. All branches cross at $M = 0$ and $\alpha = 0$. At this point the beam is straight. Figure 3.13 and 3.14 show the beam shapes corresponding to the points in figure 3.12. The points on the branch corresponding to $\dfrac{P}{P_c} = 0.8$ are shown in figure 3.13 and figure 3.14 shows the beam shapes for the point on the branch corresponding to $\frac{P}{P_c} = 1.2$.

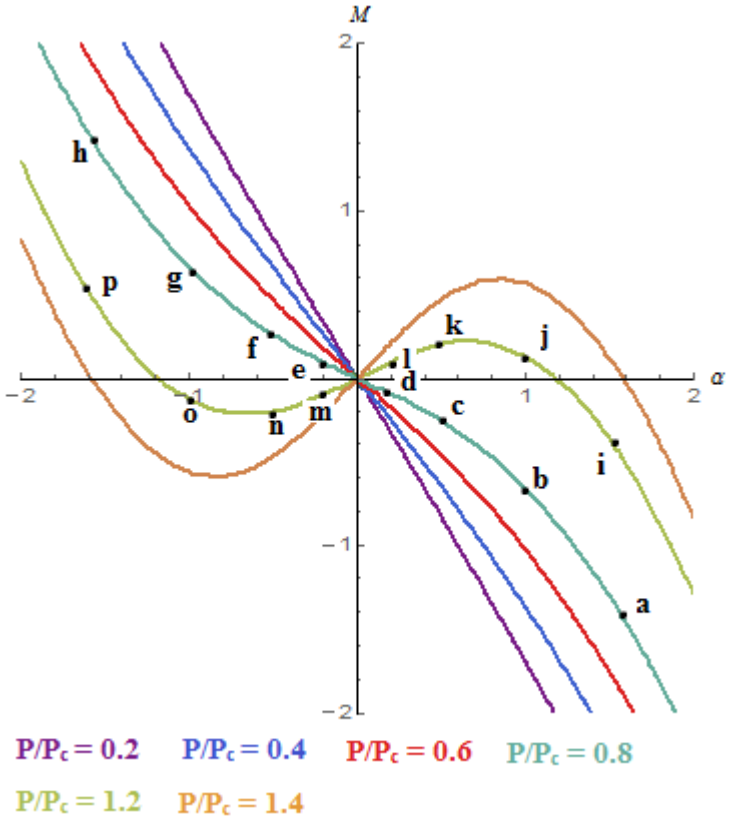

Figure 3.12: *M versus α for different values of P. All branches cross at the origin, at this point the beam is straight. The points on the branch of $\frac{P}{P_c} = 0.8$ correspond to the beam shapes in figure 3.13 and the points on the branch of $\frac{P}{P_c} = 1.2$ correspond to the beam shapes in figure 3.14.*

When we follow the branch corresponding to $\frac{P}{P_c} = 0.8$ and start from small α the beam is located in the lower half plane and has a large deflection, see beam shape a in figure 3.13. If we increase α the deflection of the beam gets smaller until $\alpha = 0$, see beam shapes b, c and d in figure 3.13. At $\alpha = 0$ the beam is flat, because M is also zero. If α is increased further the beam is located in the upper half plane and the deflection becomes larger with increasing α, see beam shape e, f, g and h in figure 3.13. For this branch all beam shapes have a monotonic θ. So if α is positive the curvature is negative and if α is negative the curvature is positive.

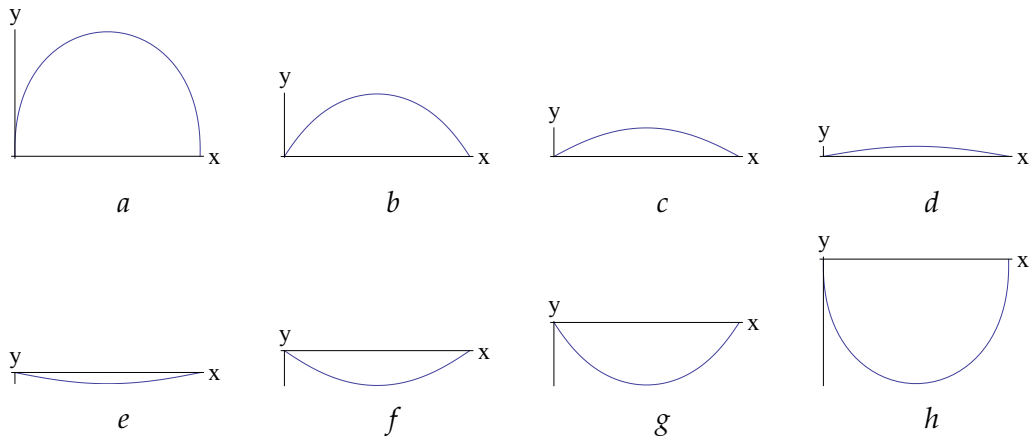

Figure 3.13: *Beam shapes corresponding to the points in figure 1.9 for $\frac{P}{P_c} = 1.2$. The more M departs from zero the larger the deflection of the beam. θ is monotonic.*

When we now follow the branch corresponding to $\dfrac{P}{P_c} = 1.2$ the beam is still more deflected if M departs more from zero, see figure 3.14. Beam shape i, and p correspond to monotonic θ. However now beam shapes j, k, l, m, n and o in figure 3.14 correspond to non-monotonic θ. Although this is not easy to see by looking at the beam shapes, for M, α positive θ first increases and then decreases and for M, α negative θ first decreases and then increases.

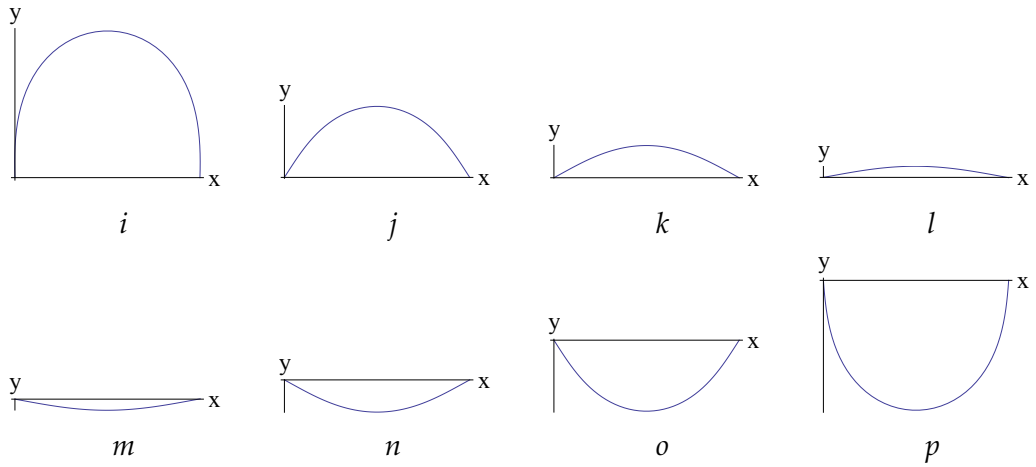

Figure 3.14: *Beam shapes corresponding to the points in figure 3.12 for $\frac{P}{P_c} = 1.2$. θ is monotonic for beam shape i and p and non-monotonic for the other beam shapes.*

3.3.3 Snapping

A branch for fixed P in the (M, α)-diagram can be followed in two different ways. We can impose α and let M change or impose M and let α change. For $P < P_c$ all points in the (M, α)-diagram can be reached and both ways of following a branch give the same result. However when $P > P_c$ the two methods give different results. If we impose α and let M change, still all points in the diagram can be reached. But if we impose M and let α change, not all points in the (M, α)-diagram can be reached. In section 4.3.2 of chapter 4 about stability we will explain why not every point can be reached. When we start from low M, and increase M at a certain point M reaches a local maximum, point a in figure 3.15. When we increase M further there is no nearby equilibrium state and the system will go to point b in figure 3.15. Looking at beam shapes we see that when the beam goes from a to b it instantly changes its curvature from non-monotonic to monotonic θ. This phenomena is called snapping. The same process happens when we start from high M and let M decrease. This can be seen in figure 3.15. The part between the local minimum and the local maximum is never reached, point a and c in figure 3.15. Imposing M and following the branch starting at low M gives a different path along the branch than following the branch and starting at hight M. This means that the followed path along the (M, α)-diagram depends on the past. So we have memory in the system, this is called hysteresis.

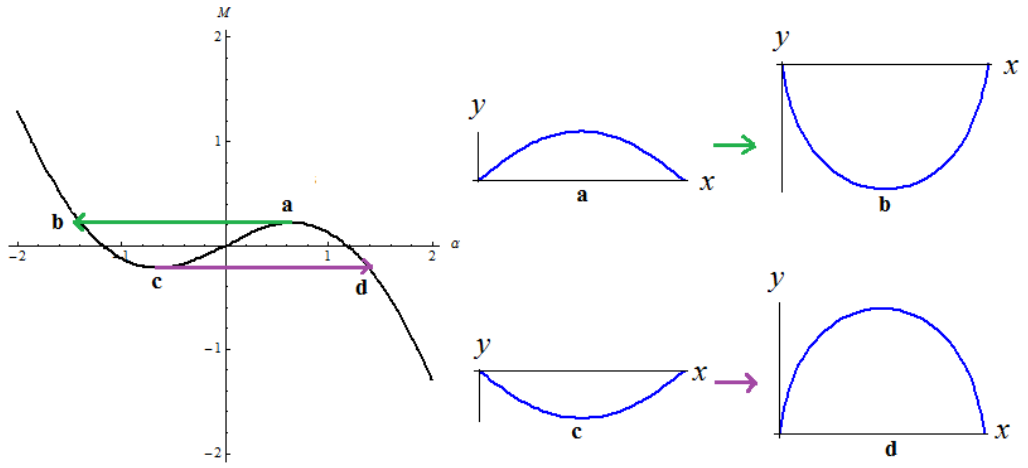

Figure 3.15: *Snapping and hysteresis. If M is imposed the beam snaps from point a to point b and from point c to point d. This snapping results in hysterese.*

3.3.4 (M, α)-diagram for higher forces

In the previous sections we only considered forces just above and below P_c. Figure 3.16 shows the (M, α)-diagram for higher forces. Figure 3.17 shows the beam shapes corresponding to the points in figure 3.16. All points on these branches correspond to beams that are in a higher mode. Again we see that the more α departs from zero, the more the beam is deflected. Figure 3.16 looks very similar to figure 3.12, therefore snapping also occurs for higher forces. When we zoom out we see the branches have a twisted shape, as shown in figure 3.18. Figure 3.16 also shows beam shapes corresponding to point a and b on the branches. The beams form loops. We do not expect that real beams take these shapes for a three-dimensional problem this is possible but that is outside the scope of this thesis. Therefore we focus on low M.

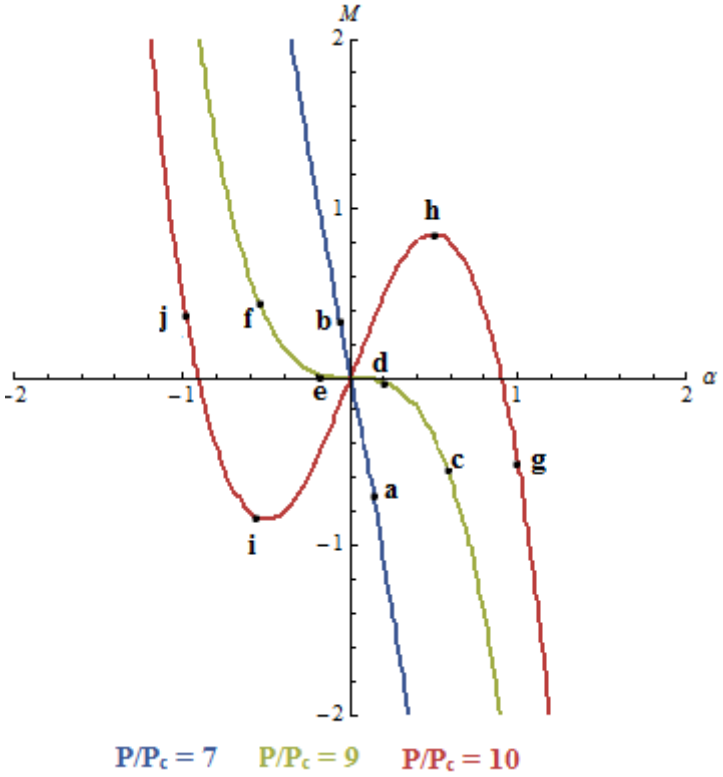

Figure 3.16: *(M, α)-diagram for forces around $P = 9P_c$. The branches look similar to the branches for P around P_c. The point on the branches correspond to the beam shapes in figure 3.17*

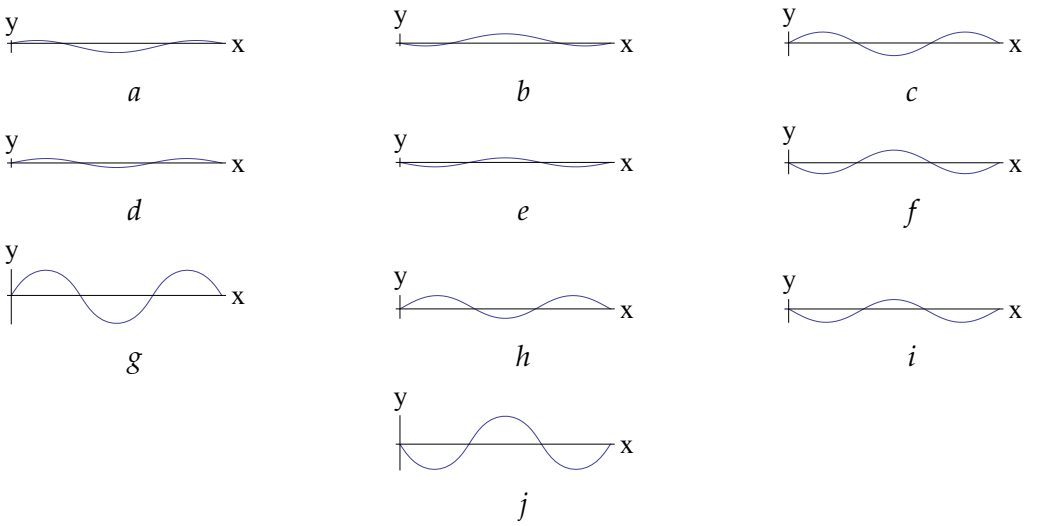

Figure 3.17: *Beam shapes corresponding to the points in figure 3.16. The beams are in the third mode. The more M and α depart from zero the larger the deflection of the beam.*

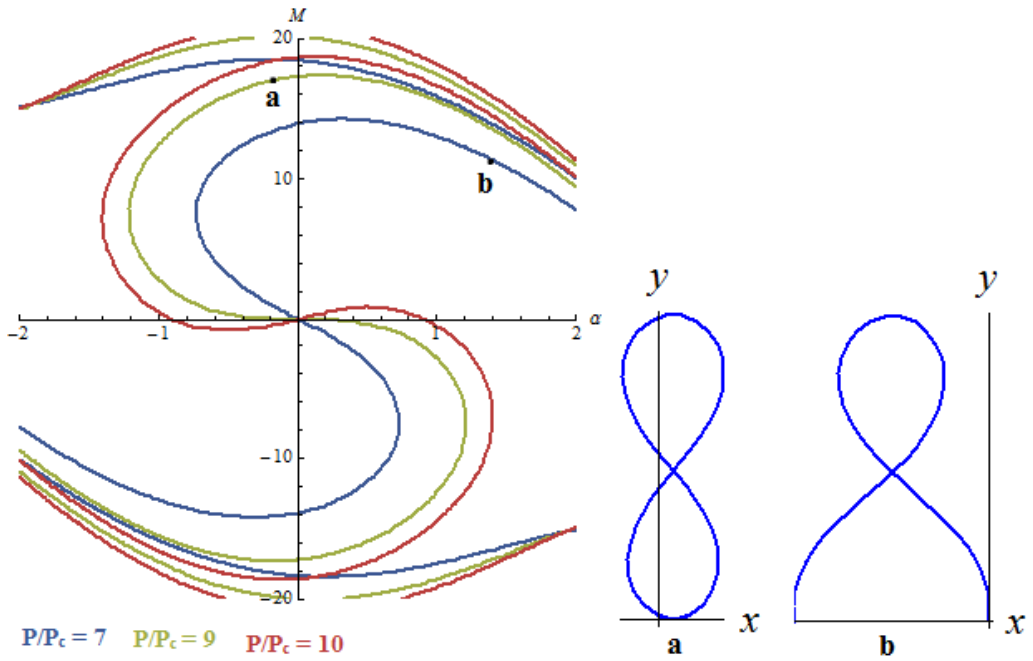

Figure 3.18: *(M,α)-diagram with beam shapes for large M. The point on the (M,α)-diagram correspond to the beam shapes. The branches have a twisted shape. The beams form loops for high M.*

3.4 3D-plot of P, M and α

Until now we studied two-dimensional projections of a three-dimensional problem. In this section we will make 3D-plots to see how these two-dimensional projections come together in a 3D-plot and to see the relation between M, P and α from different angles. Figure 3.19 shows a 3D-plot of M, P and α for P just above the critical force. Around $M = 0$ we see a gap. This is probably due to a failure in the numerics for small M. In figure 3.19a the (M, α)-diagram is visible. Figure 3.19b shows the 3D-plot from a different angle and the force is in this figure scaled by P_c, here the unfolding pitchfork bifurcation is visible.

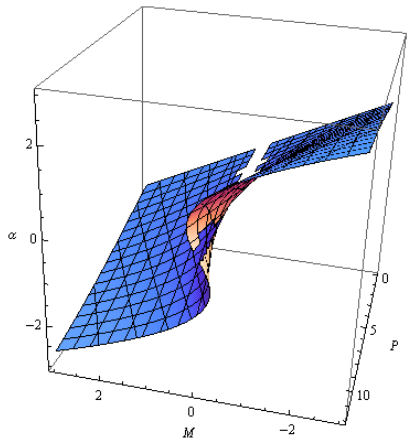

a *View on the α, M-side. Therefore the (M, α)-diagram is visible. With M on the horizontal axis and α on the vertical axis.*

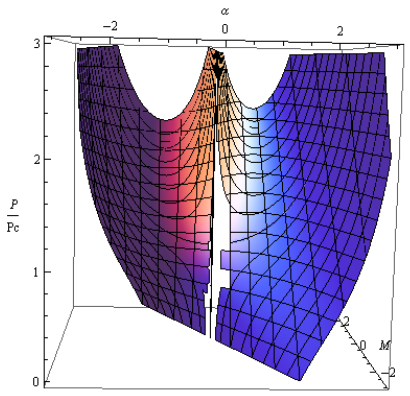

b *View on the (P, α)-side. The unfolding pitchfork bifurcation is visible.*

Figure 3.19: *3D-plot for P around P_c from two different angles.*

Figure 3.20 shows the 3D-plot for higher values of P from different angles. In figure 3.20a the multiple unfolding pitchfork bifurcations are visible and in 3.20b the (M, α)-diagram is visible. Together with figure 3.20c we see that we have three times the shape figure 3.19 and all three are connected.

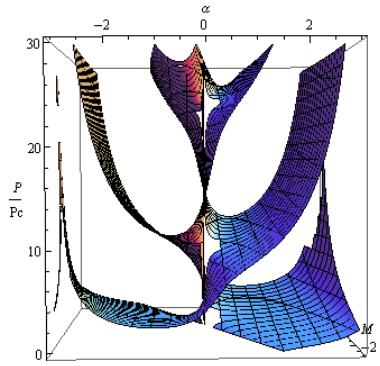

a *3D-plot from the (P, α)-side. The multiple unfolding pitchfork bifurcations are visible.*

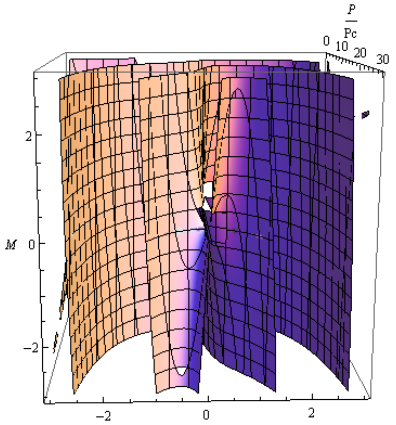

b *3D-plot from the (M, α)-side. The (M, α)-diagram is visible.*

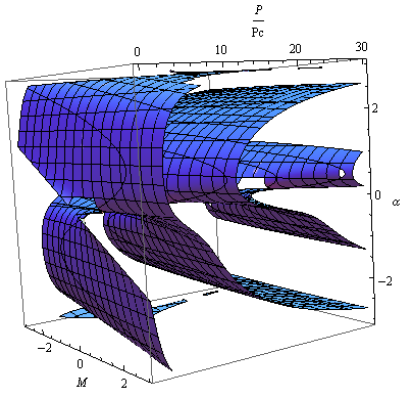

c *3D-plot viewed from another angle.*

Figure 3.20: *3D-plot up to and including the third unfolding, shown from three different angles. The (P, α)- and (M, α)-diagrams are visible. We see three times the shape of figure 3.19 and all three are connected.*

Chapter 4

Stability

To understand which beam shapes are stable and which are not, we want to analyse the stability of branches in the (P, α)-diagram and in the (M, α)-diagram. The branches in these diagrams are branches of static equilibrium, therefore each point at the branch is called a stationary point. All stationary points correspond to local minima or maxima in the potential energy. A minimum in the potential energy corresponds to a stable state and a maximum corresponds to an unstable state [16]. Each stationary point corresponds to an unique combination of P, M and α. To these values of P, M and α corresponds a beam shape. A beam is stable if the beam goes back to its initial position after applying a small perturbation and unstable if the beam switches to another state after a small perturbation.

4.1 Second variation of the potential energy

An usual approach of determining stability in discrete systems is calculating the second variation of the potential energy for each degree of freedom. For the beams we study, the degrees of freedom are θ and θ_t. Then according to the Lagrange-Dirichlet theorem, the equilibrium state is stable if the second variation of the potential energy is positive for any variation of the initial position, which means that the potential energy has a local minimum at the stationary point [15]. According to Liapunov's stability theorem a point of the branch is unstable if for any variation of the initial position the second variation of the potential energy is negative. This means the potential energy has a local maximum at the stationary point [15]. So when we want to know which beam shapes are stable, we have to check the sign of the second variation of the potential energy. For

discrete systems a static equilibrium is stable if and only if the second variation of the potential energy is non-negative. For a continuous system a non-negative second variation of the potential energy is still a necessary condition for stability but it is no longer sufficient, because the second variation is no longer necessarily dominant over the higher order variations. The second variation remains dominant for most systems. But determining stability would still be hard since we have to use Fréchet derivatives [16]. This is beyond the scope of this thesis. Therefore we have to search for other methods.

4.2 Determining stability by plotting the potential energy versus α.

First we naively try to determine the stability of the branches. Instead of calculating the second variation of the potential energy, we determine the stability of the branches by plotting the potential energy versus α for fixed M and P. Then we determine whether the energy has a local minimum or a local maximum at the branch. We use the dimensionless potential energy which is given by

$$\Lambda = \frac{E_{el}}{EI} - P(1 - \Delta u) = \frac{1}{2}\int_0^1 \theta_t^2 dt - P\left(1 - \int_0^1 \cos(\theta) dt\right). \tag{4.1}$$

For the calculation of the potential energy we use the solution of θ. This means we only consider the static equilibrium states in the calculation of the potential energy. Therefore only the values very close to the minima and maxima of the energy give useful information about the energy. A branch is at a local maximum if the curvature is positive and at a local minimum if the curvature is negative. So negative curvature means that the branch is stable and positive curvature means that the branch is unstable. Figure 4.1 shows potential energy diagrams and the stability of the branches determined in this way. Diagrams *a*,*d* and *f* have a positive curvature at the stationary point they correspond to, so at these points the beam shapes are unstable. For diagram *f* it is hard to see. However, we have checked it with the numerical values. Diagrams *b*, *c* and *e* have a negative curvature at the stationary point, therefore they are stable. The beginning of the lower left branch is unstable. This is strange because physically one would expect that a just bent beam is stable. The changing stability along the higher branches is also curious. When we look at the potential energy diagrams we see that most of the time the maximum or

minimum does not coincide with the stationary point the diagram corresponds to, see energy diagram *a*, *b* and *d* of figure 4.1. Therefore determining stability in this way is probably wrong.

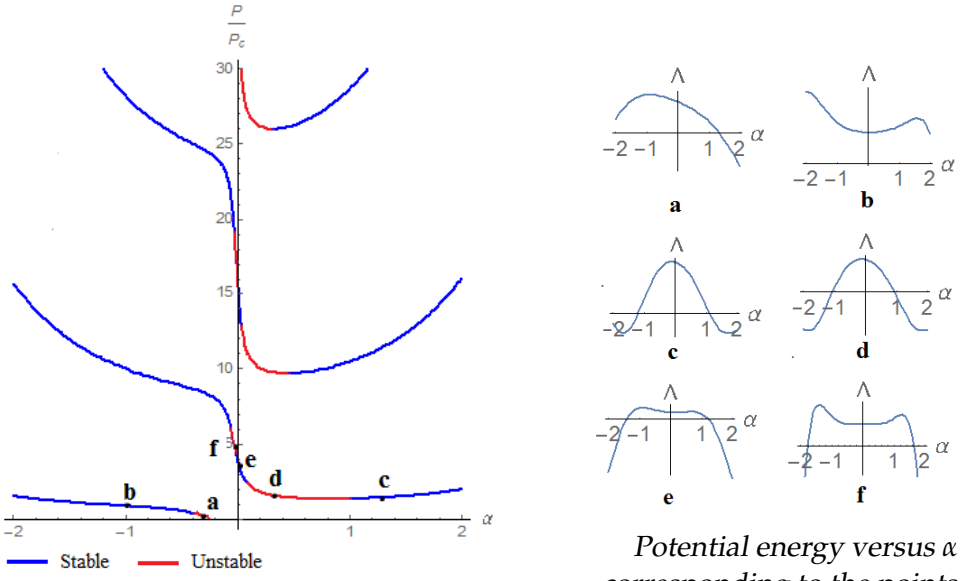

$\frac{P}{P_c}, \alpha$-diagram with stabilities.

Potential energy versus α corresponding to the points in the $\frac{P}{P_c}, \alpha$-diagram.

Figure 4.1: *Stabilities determined by plotting the potential energy versus α for $M = 0.5$. A negative curvature in the potential energy diagram corresponds to a stable branch and a positive curvature corresponds to an unstable branch.*

4.3 Determining stability using standard bifurcations

Since determining the stability analytically or numerically is beyond the scope of this thesis, we use knowledge from literature about standard bifurcations.

4.3.1 Stability of unfolding pitchfork bifurcations

For $M = 0$ we found Euler buckling. For Euler buckling the stabilities are well defined. Figure 4.2 shows the stabilities for the standard pitchfork bifurcation and the standard unfolded pitchfork bifurcation. A solid line corresponds to a stable branch and a dashed line to an unstable branch.

The parameter $\overline{x}$ corresponds to α and d corresponds to P, $d = 0$ corresponds to P_c [17].

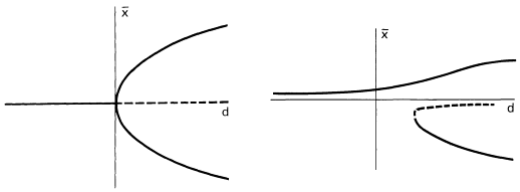

Figure 4.2: *On the left a standard pitchfork bifurcation and on the right a standard unfolded pitchfork bifurcation, $\overline{x}$ corresponds to α and d to P. A solid line corresponds to a stable branch and a dashed line to an unstable branch [17].*

Since $M = 0$ gives a standard pitchfork bifurcation, we suppose that for $M \neq 0$ the unfolded pitchfork bifurcation corresponds to a standard unfolded pitchfork bifurcation. Figure 4.3 shows the resulting stabilities. For $P < P_{Euler}(\alpha)$ all beam shapes are stable and for $P > P_{Euler}(\alpha)$ beams with a larger deflection are stable and beams with a smaller deflection are unstable.

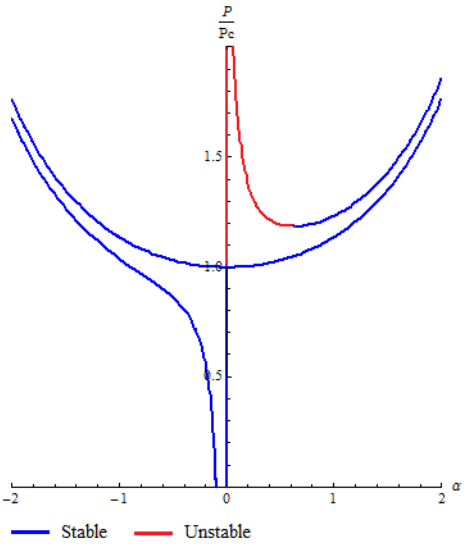

(P, α)-diagram with stabilities for $M = 0$ and $M = 0.5$.

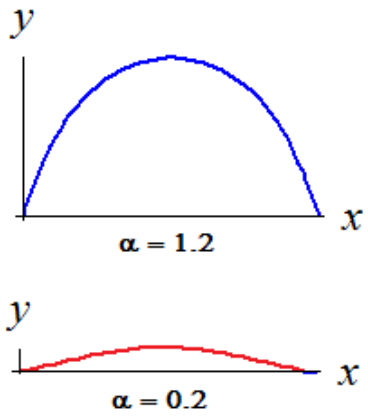

Stable and unstable beam shapes for $P > P_{Euler}(\alpha)$ and $M = 0.5$.

Figure 4.3: *Stabilities determined by a standard unfolded pitchfork bifurcation. For $P < P_{Euler}(\alpha)$ all beam shapes are stable and for $P > P_{Euler}(\alpha)$ beams with a small deflection are unstable and beams with a larger deflection are stable.*

4.3.2 Hysteresis

Figure 4.4 shows the standard bifurcations for the (M, α)-diagram. These bifurcations are saddle-node bifurcations, in figure 4.4 denoted as SN. The solid line means stable and the striped line means unstable. The parameter x corresponds to α, h corresponds to M and μ to P. So $\mu = 0$ corresponds to P_c. The arrows are directed towards the stable branches. For $\mu < 0$ the whole branch is stable and for $\mu > 0$ only part of the branch is stable. The branch is unstable for small x and stable for larger x. The unstable part lies between the two saddle-nodes. If we start at low h and increase h following the equilibrium branch then as soon as we reach the saddle-node there is no nearby equilibrium state. So the structure snaps to an equilibrium state elsewhere on the curve, the system follows the long arrow in figure 4.4. This is similar to the snapping of a beam. If we start at high h and lower h until we reach the saddle point the behaviour is similar. Therefore the path of the structure depends on the past so there is hysteresis in the system [18].

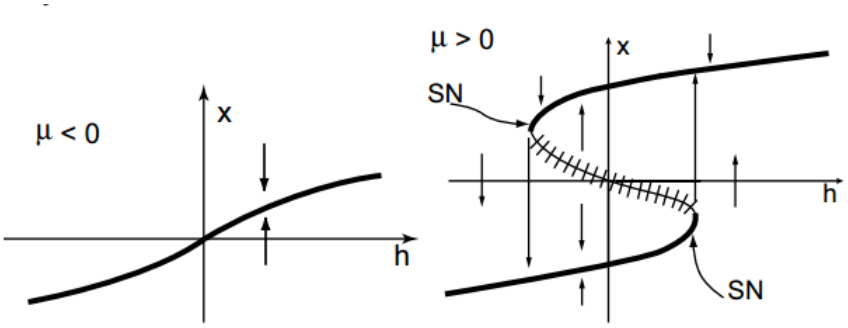

Figure 4.4: *Standard stabilities and hysteresis, x corresponds to α and h to M. Solid line is stable and striped line is unstable. The saddle-node bifurcations are denoted by SN [18].*

Since the (M, α)-diagram is just another two-dimensional projection of a three-dimensional problem the bifurcations in the (M, α)-diagram probably correspond to the standard saddle-node bifurcations. Figure 4.5 shows the resulting stabilities and the corresponding beam shapes. For $P < P_c$ all beam shapes are stable and for $P > P_c$ beams with a larger delflection are stable and beams with a smaller deflection are unstable, so the results from the (P, α)- and the (M, α)-diagram correspond with each other. As discussed for the standard bifurcation the red part in figure 4.5 will never be reached. Snapping and hysteresis originate in saddle-node bifurcations, which themselves are induced by the unfolded pitchfork bifurcation. This

gives the explanation for the snapping and hysteresis we discussed in section 3.3.3.

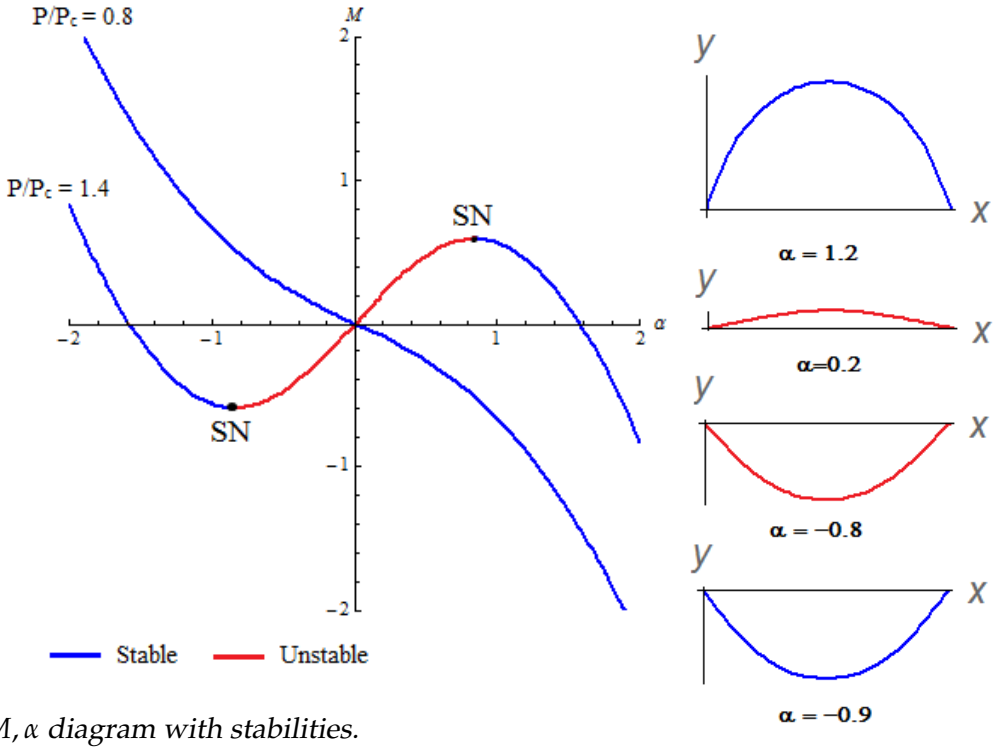

M, α diagram with stabilities. The saddle-node bifurcations are denoted by SN.

Stable and unstable beam shapes $P > P_c$.

Figure 4.5: *Stabilities determined by standard bifurcations. Beams with a small deflection are unstable and beams with a larger deflection are stable. Hysteresis and snapping originate in the saddle-node bifurcations.*

4.3.3 Cusp catastrophe

We have studied the stabilities of two dimensional projections of our three dimensional problem. The 3D-plot up to and including the first unfolding, figure 3.19 looks very similar to a cusp catastrophe, shown in the upper left picture of figure 4.6 [2]. Except for the gap for small M, which is due to a numerical failure. In figure 4.6 θ corresponds to α, μ to P and ϵ to M. The stabilities shown in the upper left picture correspond to the stabilities we found for the (M, α)-diagram in section 4.3.2. The figure also shows that when we take slices by taking ϵ constant we get an unfolding pitchfork bifurcation. Taking slices in the (P, α)-diagram for constant M also gives

an unfolding pitchfork bifurcation, as we have seen in section 4.3.1. The projection on the $\epsilon - \mu$ space shows the positions of the saddle-node bifurcations. To be certain that the 3D-plot in figure 3.19 is a cusp catastrophe we have to determine the position of the saddle-node bifurcations. For this a computation of the stabilities is needed. This is beyond the scope of this these and therefore we leave it for further research.

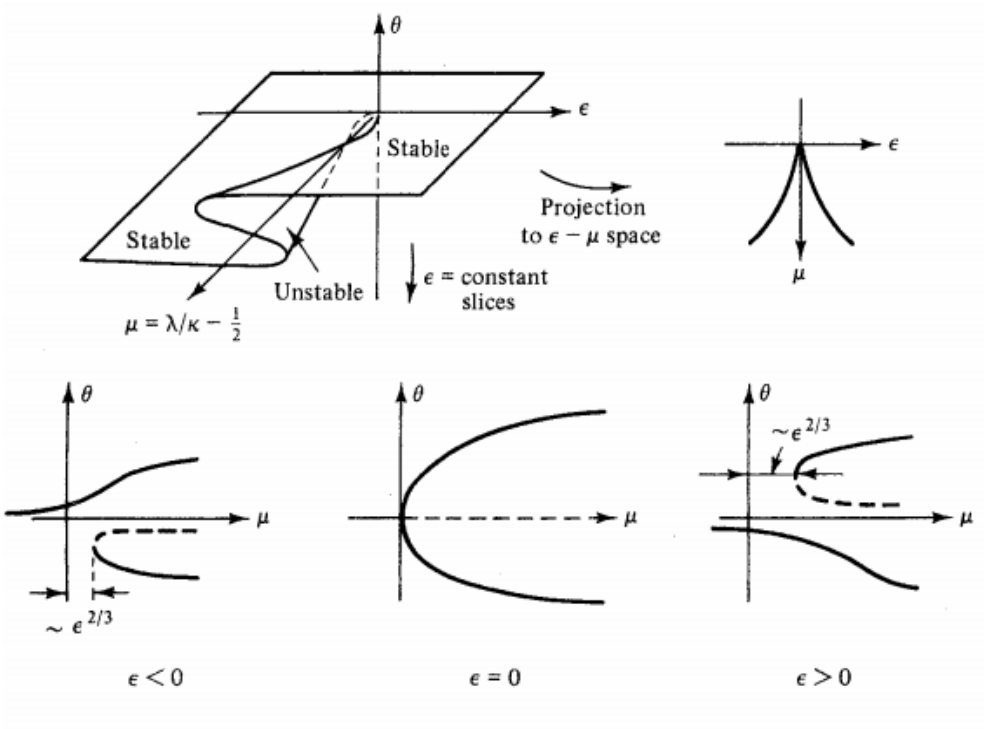

Figure 4.6: *Cusp catastrophe θ corresponds to α, μ to P and ϵ to M. In the 3D-picture the stabilities are written. For the 2D-projection a solid line is stable and a dashed line is unstable. The μ, ϵ-diagram shows the position of the saddle-node bifurcations. [2]. The θ, μ-diagram contains a pitchfork bifurcation and unfolded pitchfork bifurcations.*

4.3.4 Stabilities for higher forces

Literature provides us to determine the stability of the equilibrium branches up to and including the first unfolding, as we have seen in the previous sections. Each time $P = (2n+1)^2 P_c$, $n \in \mathbb{N}$ we find an unfolding pitchfork bifurcation. We suppose these bifurcations correspond to standard bifurcations, from which we deduce the stability. However, at this point

it is unknown how these pitchforks are connected, even for Euler buckling literature does not provide the stability of the connections. Figure 4.7 shows the resulting stabilities and the corresponding beam shapes. The blue lines are stable, the red unstable and for the green lines the stability is unknown. We see that for $P > P_{Euler}(\alpha)$ beam shapes with a small deflection either are stable or their stability is unknown. In contrast, beams with a larger deflection are stable.

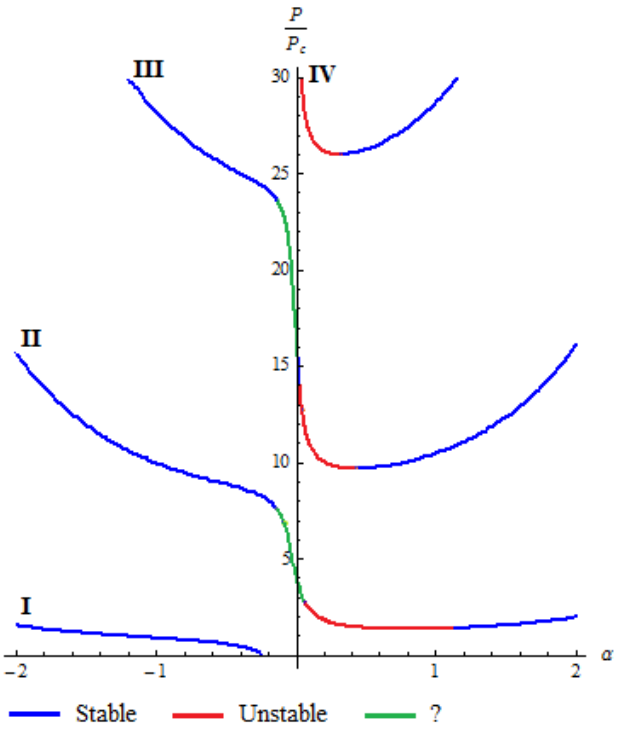

$\frac{P}{P_c}, \alpha$-diagram with stabilities.

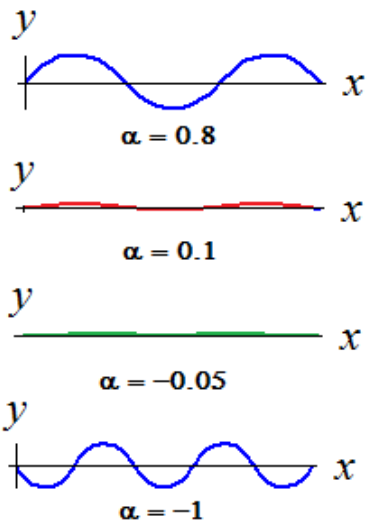

Stable and unstable beam shapes for branch III.

Figure 4.7: *Stabilities determined by standard bifurcations. Branch one is stable. Branch II and III are partly stable and for the connections between the bifurcations the stability is unknown. Branch IV is partly stable and partly unstable. Beams with a small deflection are either stable or their stability is unknown. Beams with a larger deflection are stable.*

Figure 3.16 showed a (M, α)-diagram for higher values of P which looked very similar to the (M, α)-diagram for values of P around P_c. However figure 3.18 showed that when we zoom out, the branches get twisting shapes, so M gets multivalued for fixed α. Therefore we cannot use this to determine the stability from standard bifurcations. However, since the (P, α)-diagram consists of multiple connected unfolding pitchfork bifurcations

at $P = (2n+1)^2 P_c$, $n \in \mathbb{N}$ and an unfolded pitchfork bifurcation induces saddle-node bifurcations, we suspect to have stabilities corresponding to standard bifurcations for the (M, α)-diagram for values of P around $P = (2n+1)^2 P_c$, $n \in \mathbb{N}$ as long as we consider small M. The saddle-node bifurcations cause the snapping and hysteresis.

The 3D-plot for higher values of P in figure 3.20 seems to consist of connected cusp catastrophes. The (P, α)-diagram consists of multiple connected unfolding pitchfork bifurcations at $P = (2n+1)^2 P_c$, $n \in \mathbb{N}$ and around these value of P we alse have stabilities corresponding to standard stabilities in the (M, α)-diagram. Again, to be certain that the 3D-plot in figure 3.20 consists of connected cusp catastrophes we have to determine the position of the saddle-node bifurcations. For this a computation of the stabilities is needed. This is beyond the scope of this these and therefore we leave it for further research.

4.4 Approximation by a discrete system

Determining stability in a continuous system is hard, as explained in section 4.1, therefore an usual approach to determine the stability is to approximate the continuous system by a discrete system [19]. Figure 4.8 shows a picture of a beam and a discrete beam. First we show a simple model to describe buckling and then we explain how the problem we are dealing with can be approximated by discrete systems.

Figure 4.8: *A continuous and a discrete beam.*

4.4.1 Two bars connected by a torsion spring

The most easy example to describe buckling is connecting two bars by a torsional spring. For the derivation of the differential equation and its solution we follow "Simple buckling model" by C. Coulais and L. Lubbers

[20]. Consider two bars of length $\frac{1}{2}$ connected by a torsion spring with spring constant K. Let θ be the angle between the two bars. First we derive the equation for this problem by minimization of the energy, similar to what we did for the beam in section 2.4.2. The energy of the spring is given by

$$E = \frac{1}{2}K\theta^2. \tag{4.2}$$

As for the beam we have to minimize the energy under the constraint

$$\Delta u = 1 - \cos(\theta). \tag{4.3}$$

Again the Lagrange multiplier is the applied force P. Then the Lagrangian is given by

$$\Lambda = \frac{1}{2}K\theta^2 + P\left(\Delta u - (1 - \cos(\theta))\right). \tag{4.4}$$

Energy minimization gives

$$\delta E = \frac{\partial \Lambda}{\partial \theta} = K\theta - P\sin(\theta) = 0. \tag{4.5}$$

Therefore we have the nonlinear homogeneous algebraic equation

$$K\theta - P\sin(\theta) = 0. \tag{4.6}$$

For small θ we can take the Taylor expansion of $\sin(\theta)$. Then the equation becomes

$$\theta\left(K - P\left((1 - \frac{\theta^2}{6}\right)\right) = 0. \tag{4.7}$$

Then the solutions are $\theta = 0$ for all P and for $P > K$ we also find the two solutions

$$\theta = \pm\sqrt{6\left(1 - \frac{K}{P}\right)}. \tag{4.8}$$

Now we will determine the stability of the solutions. We follow the method using the potential energy as described in section 4.1 . Because we are dealing with a discrete system with one degree of freedom, calculating the second variation of the potential energy is reduced to calculating the second derivative of the Lagrangian. Let V be the second derivative of the Lagrangian. Then

$$V = \frac{\partial^2 \Lambda}{\partial \theta^2} = K - P\cos(\theta). \tag{4.9}$$

First we check the stability for $\theta = 0$. Substituting $\theta = 0$ in V gives

$$V = K - P. \tag{4.10}$$

Then $V < 0$ for $P > K$ and $V > 0$ for $P < K$. So the solution $\theta = 0$ is stable for $P < K$ and unstable for $P > K$. Now we will check the stability for $\theta = \pm\sqrt{6\left(1 - \frac{K}{P}\right)}$. Therefore we first determine how the force depends on the displacement by using a Taylor expansion of the $\cos(\theta)$ [20]. This gives

$$u = (1 - \cos(\theta)) \approx \frac{\theta^2}{2} \approx 3\left(\frac{P}{K} - 1\right). \tag{4.11}$$

Therefore we can write P as

$$P = K\left(\frac{\theta^2}{6} + 1\right). \tag{4.12}$$

Substituting in V and taking the Taylor expansion of the cosine gives

$$V = K\left(\frac{\theta^4}{12} + \frac{\theta^2}{3}\right) > 0. \tag{4.13}$$

So the solutions $\theta = \pm\sqrt{6\left(1 - \frac{K}{P}\right)}$ are stable. Therefore this problem gives a pitchfork bifurcation and is the simplest way of describing buckling.

4.4.2 Discrete system

There are several ways of approximating the system by a discrete system. We can consider the continuous beam as built up of infinitely many bars connected by torsional springs. The two bars connected by a torsional spring can be extended to more bars connected by more torsional springs. Then we just have to calculate the matrix of all the variations [15]. A way to determine the stability would be taking many torsional springs and calculate numerically the variations. Another method of calculating the energy would be to discretize the system. Several methods are described in the book "Stability of discretized nonlinear elastic systems" by Lazarus et al. [19]. Since we wanted to explore how far we can push elastica in a continuous way we leave this for further research.

Chapter 5

Pre-curved beams

Until now we only considered beams without pre-curvature. In this chapter we will study pre-curved beams.

5.1 Constant pre-curvature

In section 2.4 we derived an inhomogeneous nonlinear differential equation

$$\theta_{tt} - \theta^0_{tt} + P\sin(\theta) = 0. \tag{5.1}$$

To solve this equation for a pre-curved beam we take the angle in the pre-curved beam, θ^0, to be a linear function. Let a and b be constants then the angle between the horizontal an the beam is given by $\theta^0(t) = at + b$. Note that because of the symmetry of the beam $\theta(0) = -\theta(1)$ and therefore $a = -2b$. From the assumption that θ is linear follows that the pre-curvature is given by $\theta^0_t = a$. Thus we have a constant pre-curvature. Therefore $\theta_{tt} = 0$ and we obtain the same homogeneous nonlinear differential equation as for a beam without pre-curvature. Therefore the equation is given by

$$\theta_{tt} + P\sin(\theta) = 0. \tag{5.2}$$

The difference between a beam with constant pre-curvature and a beam without pre-curvature lies in the boundary conditions, which are now given by

$$\begin{aligned} &\theta(0) = b,\ \theta(1) = -b, \\ &\theta_t(0) = M - 2b,\ \theta_t(1) = -M + 2b. \end{aligned} \tag{5.3}$$

Therefore the only change in the solution will be that α will be replaced by $\alpha + b$ and M will be replaced by $M - 2b$.

5.2 Shifted diagrams of equilibrium branches

Figure 5.1 shows that the (P, α)-diagram and the (M, α)-diagram are a shifted version of these diagrams for initially straight beams, see figure 3.5 and 3.12.

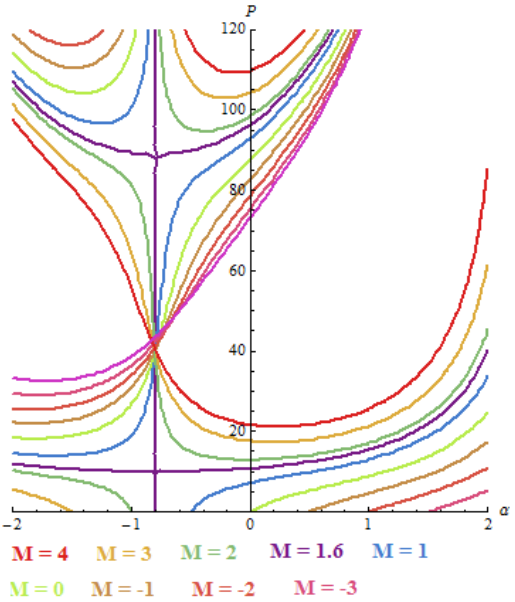

(P, α)-diagram for beams with a constant pre-curvature. Buckling is destroyed for $M = 0$ and recovered for $M = 1.6$.

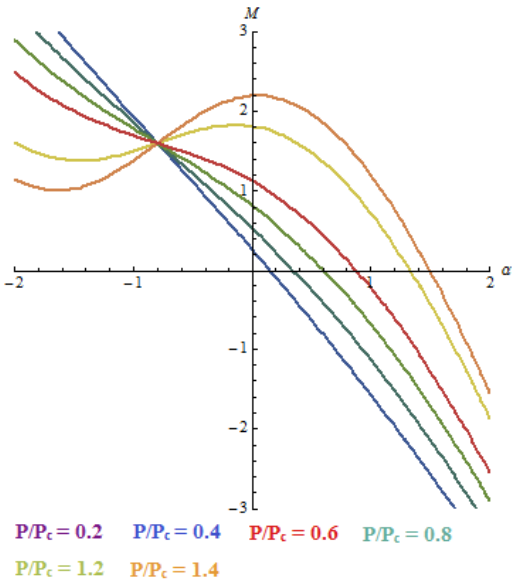

(M, α)-diagram for beams with a constant pre-curvature. The beam is flat at the crossing point of the branches, $M = 1.6$ and $\alpha = -0.8$.

Figure 5.1: *Shifted diagrams for beams with a constant pre-curvature $\theta_s^0 = -1.6$. Compared to the diagrams for an initially straight beam the (P, α)-diagram is shifted along the α-axis by an amount of $\alpha = -0.8$. The (M, α)-diagram is shifted along the M-axis by an amount of $M = 1.6$ and along the α-axis by an amount of $\alpha = -0.8$.*

In the (P, α)-diagram we see that applying a constant pre-curvature destroys the buckling for $M = 0$. The equilibrium branches corresponding with $M = 0$ are part of the unfolded pitchfork bifurcation in stead of the pitchfork bifurcation itself. Figure 5.1 shows that for a beam with a pre-curvature of $\theta_t^0 = -1.6$ buckling is recovered for $M = 1.6$. The equilibrium branch corresponding to $M = 1.6$ is the pitchfork bifurcation. In general this means that for a beam with a pre-curvature of $\theta^0 = a$ buckling is restored for $M = -a$. The diagram is only translated along the α-axis by an amount of θ_t. Therefore the unfolding pitchfork bifurcations are still at

$P = (2n+1)^2 P_c, \quad n \in \mathbb{N}.$

The (M, α)-diagram is shifted along the α- and the M-axis. The equilibrium branches are still monotonic for $P < P_c$ and non-monotonic for $P > P_c$. Therefore the snapping of a beam still occurs for values of $P > P_c$.

In the diagrams we see a shift over α and M relative to the diagrams for a beam without pre-curvature. Therefore the problem is very similar to the problem for an initially straight beam. A beam with constant pre-curvature gives just a shifted version of an initially straight beam. Buckling is still present for $M = -\theta_t^0$ and $M = 0$ corresponds to an equilibrium branch of the unfolded pitchfork bifurcation. Therefore applying a moment is like applying a pre-curvature. Consequently, for describing beams with constant pre-curvature we can use the analysis we did for an initially straight beam.

Chapter 6

Conclusion

This thesis is a study on the elastica of inextensible one-dimensional beams, with a force and a moment applied on the endpoints of the beam. The boundary conditions, we impose, require the beams to be symmetric. We described the beams by a continuous one-dimensional model, the elastica. The question we tried to answer is

> How far can we push the elastica keeping the system continuous?

The static equilibrium states of a beam can be found by energy minimization. Using the method of Lagrange we derived an inhomogeneous partial differential equation for a pre-curved beam. For beams without pre-curvature the differential equation is reduced to a homogeneous nonlinear partial differential equation, which we solved analytically. The solution of the differential equation provides an implicit equation of the force P, the moment M and the angle at the endpoints of the beam α. At a late stage of this project we found out that the derivation of the solution we used was methodologically incorrect for non-monotonic θ. Within our time limit, we could derive a second implicit solution. We suspect both solutions give the same results for both monotonic and non-monotonic θ. Then we plotted both solutions up to and including the third mode in one figure. The lines coincide. Therefore we suspect that the solutions give the same result for all modes. To be certain a transformation to rewrite one solution as the other needs to be found. Due to a lack of time we did not use the second solution in the analysis of the equilibrium branches.

Applying only a force and no moment provides the possibility to analytically determine an explicit equation for P versus α. The result is Euler buckling with the corresponding pitchfork bifurcation at $P = P_c$. When $M \neq 0$ we explore the implicit equation by plotting two-dimensional projections of the three-dimensional problem.

Applying a moment breaks the left-right symmetry of the pitchfork bifurcation and the pitchfork bifurcation unfolds. Buckling is destroyed and the beam bends. Figure 6.1 shows multiple unfolded pitchfork bifurcations, with bent beams. For each point on the equilibrium branch the beam shape can be determined plotted. Due to the symmetry breaking, applying a moment gives a preference for a bending direction. The bending direction depends on the sign of the moment. The deflection is monotonic for beams at branch I, see beam shape *a*. For higher forces the beam's deflection is non-monotonic and the endpoints rotate into the opposite direction. This is shown by beam shapes *b* and *c*. When the force is increased further the beam deforms into a higher mode. Each time $P = (2n+1)^2 P_c$ with $n = 0, 1, 2, ..$ we find an unfolding pitchfork bifurcation. Figure 6.1 shows three unfolded pitchfork bifurcations in the (P, α)-diagram.

Taking the force constant gives the possibility to determine the equilibrium branches in the (M, α)-diagram. This relation is monotonic for $P < P_c$ and non-monotonic for $P > P_c$, as shown in figure 6.1. Also for the (M, α)-diagram the beam shape can be determined plotted for each point on the equilibrium diagram. The more M and α depart from zero, the larger the deflection of the beam.

Determining stability in a continuous system requires techniques that are beyond the scope of this thesis. We suppose that our bifurcations correspond to standard bifurcations in literature, from which the stabilities can be deduced. The stabilities are shown in figure 6.1. The blue branches correspond to stable branches and the red branches to unstable branches. The stability of the connections between pitchforks is unknown in literature. Therefore the stability of the green branches is unknown. Beams with a small deflection either are stable or their stability is unknown. In contrast beams with a larger deflection are stable. In figure 6.1 a number of beams with their stability are shown.

In the (M, α)-diagram branches for $P < P_c$ are stable and branches for P just above P_c have two saddle-node bifurcations. The part of the branch

between these saddle-nodes is unstable, see the red part in the (M, α)-diagrams in figure 6.1. Hysteresis in the system and snapping of the beam originate in the saddle-node bifurcations. When a beam snaps it instantly changes its curvature. We suppose the branches in the (M, α)-diagram for forces around $P = (2n+1)^2 P_c$, $n = 0, 1, 2, ...$ all have the same stability. For the intermediate forces the stability is unknown in literature.

The combination of the stabilities in the (P, α)- and (M, α)-diagrams and the form of 3D-plots suggests that the system undergoes a sequence of cusp catastrophes.

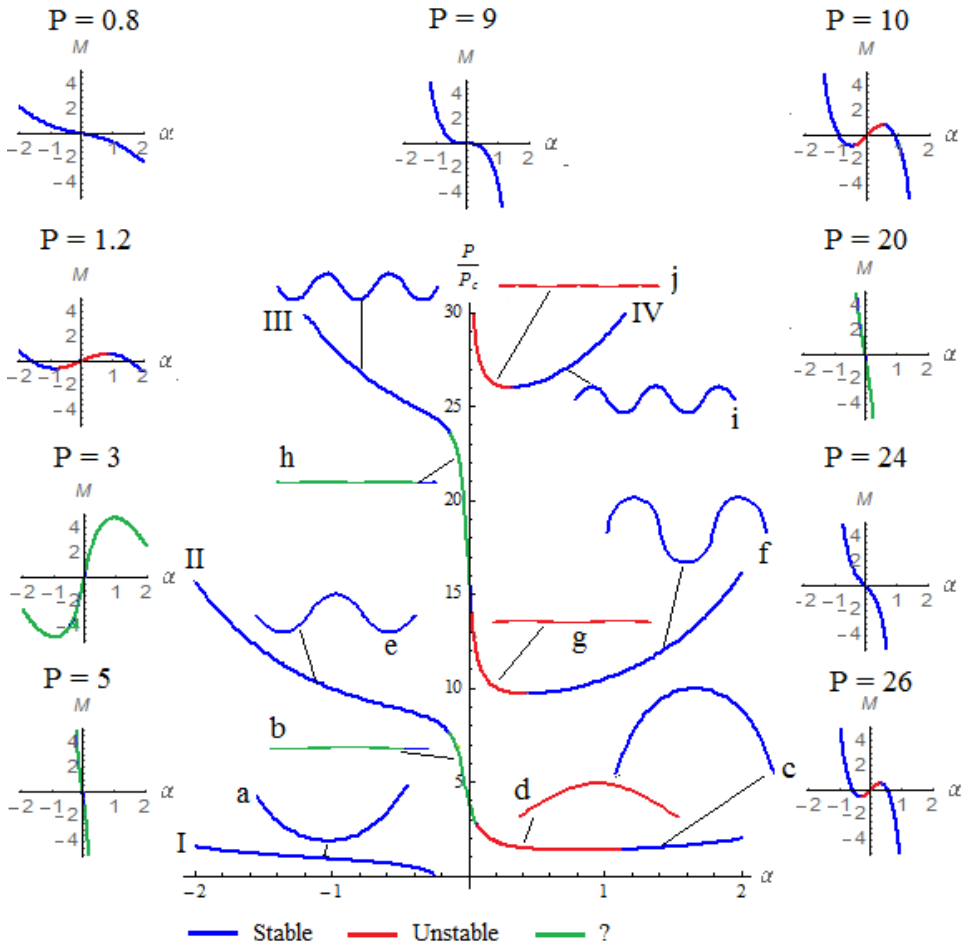

Figure 6.1: *Multiple unfolded pitchfork bifurcations for $M = 0.5$ with stabilities. Beam shapes with stabilities. Moment angle diagrams for several values of P, with stabilities. The branches in the (P, α)-diagram are labeled by Roman numerals and the beam shapes by letters.*

Finally we investigated the effect of applying a constant pre-curvature. A beam with a constant pre-curvature has the same differential equation as an initially straight beam. Only the boundary conditions are different. This difference causes a shift in the (P, α)- and (M, α)-diagrams. Applying a pre-curvature destroys buckling for zero moment and buckling can be restored by applying a moment. A constant pre-curvature gives a similar but shifted problem. Therefore, applying a moment is like applying a constant pre-curvature.

Running to the question 'How far can we push the elastica keeping the system continuous?', the answer is as follows. We can determine the equilibrium branches of P, M and α and we can plot corresponding beam shapes for initially straight beams and beams with a constant pre-curvature. More research needs to be done on the recently found solution. Either by verifying that the two approaches are the same or by exploring new results. Calculating the stability is beyond the scope of this thesis. Therefore we refer to the literature to determine the stabilities of the bifurcations. However, what we could not determine, is the stability of the connection between the bifurcations. Figure 6.1 gives an overview. For further research it would be interesting to calculate the stability either with advanced mathematical techniques or by approximating the system by a discrete system.

Chapter 7

Acknowledgements

Writing a thesis is a group project, ranging from having a headache from not knowing what to write to enjoying a "Christmas tree" together. Therefore while having trouble deciding in what style to write, it quickly turned plural. We calculate; we see; we search, sometimes in vain, in literature.

The first calculations that I saw, were from Willem Schouten, my predecessor. Being allowed to continue his work, was a great feeling. A greenhorn, that is what I was. I could always turn to Corentin Coulais and Luuk Lubbers for advice and have gotten amazing feedback from them. Seldom have I learned this much. The moment my understanding of the mathematical side of the project stopped, Vivi Rottschäfer was there to willingly aid me and push me in the right direction. This meant racking my brain quite often. And there was Martin van Hecke, weekly present at the discussion of the research group, giving insight how to continue the project.

There was some pressure at the end. Receiving the request to hand in a draft of the thesis, was the moment sleeping was no longer an option. However this was all worth it, because it meant taking the next step.

Working on this research has been a huge pleasure for me. Never could I have guessed that I could put so much of my time and attention into a beam, without the slightest thought of boredom on my mind. On the contrary, I will miss it! Not only the research, but also the team, the people who helped me and my roommates. Hereby I declare my upmost gratitude to all of you for this amazing experience.

Mara

References

[1] R. Levien, *The elastica: a mathematical history*, Technical Report UCB/EECS-2008-103, EECS Department, University of California, Berkeley, 2008.

[2] J. E. Marsden and T. J. Hughes, *Mathematical foundations of elasticity*, Dover publications, INC., New York, 1994.

[3] T. Mullin, S. Deschanel, K. Bertoldi, and M. Boyce, *Pattern transformation triggered by deformation*, Physical review letters **99**, 084301 (2007).

[4] J. M. Gere and B. J. Goodno, *Mechanics of materials*, Cengage Learning, Stamford, 8 edition, 2012.

[5] K. Bertoldi, P. M. Reis, S. Willshaw, and T. Mullin, *Negative Poisson's ratio behavior induced by an elastic instability*, Advanced Materials **22**, 361 (2009).

[6] B. Florijn, C. Coulais, and M. van Hecke, *Programmable mechanical metamaterials*, Physical review letters **113**, 175503 (2014).

[7] H. Nowacki, M. Bloor, and B. Oleksiewicz, *Computational geometry for ships*, World scientific Co. Pte. Ltd, Singapore, 1995.

[8] H. D. Young, R. A. Freedman, and L. Ford, *Sears and Zemansky's university physics*, Pearson education, 2004.

[9] G. R. Fowles and G. L. Cassiday, *Analytical mechanics*, Thomson Brooks/cole, Belmont, 2005.

[10] W. Schouten, *Elastic instabilities in monoholar and biholar patterned networks*, 2014.

[11] A. Váquez, C. Villabos, D. Alcaranaz, T. Vázquez, and C. López, *Exact solution for the nonlinear pendulum*, Revista Brasileira de Ensino de Físíca **29**, 645 (2007).

[12] M. Abramowitz and I. A. Stegun, *Handbook of mathematical functions: With Formulas, Graphs, and Mathematical Tables*, Number 55, National Bureau of Standards Applied Mathematics, 1964.

[13] R. A. Adams and C. Essex, *Calculus a complete course*, 2010.

[14] *Wolfram*, `http://functions.wolfram.com/EllipticIntegrals/`.

[15] Z. P. Bažant and L. Cedolin, *Stability of structures, Elastic, Inelastic, Fracture and Damage Theories*, World Scientific Publishing Co. Pte. LTd., Singapore, 2010.

[16] J. W. H. D. D. J. Bernard Budiansky, S.C. Cowin and K. Stewartson, *Advances in applied mechanics*, Academic Press. Inc., New York, 1974.

[17] J. Hale and H. Koçak, *Dynamics and Bifurcations*, Springer-Verlag, New York, 1991.

[18] H. Riecke, *Methods of Nonlinear Analysis 412*, Technical report, Northwestern University, 2008.

[19] A. Lazarus, *Energy minimization and dynamical systems*, in *Stability of discretized nonlinear elastic systems*, Springer, Vienna, 2015.

[20] C. Coulais and L. Lubbers, *Simple buckling model*, Unpublished.